Material Science and Technology Division

Propulsion Materials Program
Quarterly Progress Report for
October thru December 2011

David P. Stinton
Technical Project Manager

Prepared for
U.S. Department of Energy
Assistant Secretary for Energy Efficiency and Renewable Energy
Office of Vehicle Technologies Program
VT 05 04 000

Prepared by the
OAK RIDGE NATIONAL LABORATORY
Oak Ridge, Tennessee 37831-6066
Managed by
UT-Battelle, LLC
for the Department of Energy
Under contract DE-AC05-00OR22725

CONTENTS

Project 18516 – Materials for Hybrid and Electric Drive Systems

Agreement 19201 – MBD Non-Rare Earth Magnetic Materials *(ORNL)*

Agreement 23278 - Low-Cost Direct Bonded Aluminum (DBA) Substrates *(ORNL)*

Agreement 23279 - Improved Organics for Power Electronics and Electric Motors *(ORNL)*

Project 18518 – Materials for High Efficiency Engines

Agreement 19202 – Titanium Friction and Wear *(ORNL)*

Agreement 23284 – Friction Reduction Through Surface Modification *(ORNL)*

Agreement 11752 – Materials for HCCI Engines *(ORNL)*

Agreement 13329 – Design Optimization of Piezoceramic Multilayer Actuators for Heavy Duty Diesel Engine Fuel Injectors *(ORNL)*

Agreement 17257 – Materials for Advanced Turbocharger Design *(ORNL)*

Agreement 18570 – Engine Materials Compatibility with Alternate Fuels *(ORNL)**

Agreement 18571 – Materials Issues Associated with EGR Systems *(ORNL)*

Agreement 23285 - Efficiency Implications of Advanced Materials in Advanced Combustion Internal Engines *(ORNL)*

Project 18519 – Materials for Exhaust and Energy Recovery

Agreement 9130 – Catalyst Characterization *(ORNL)**

Agreement 10461 – Durability of Diesel Engine Particulate Filters *(ORNL)**

Agreement 10635 – Catalysts via First Principles *(ORNL)*

Agreement 19214 - Biofuels Impact on Diesel Particulate Filters *(ORNL)*

Agreement 20091 – Electrically Regenerated DPF Material *(ORNL)*

<u>Project 18865 – Materials by Design</u>

Agreement 9105 – Characterization of Catalyst Microstructures *(ORNL)*

Agreement 14957 – Thermoelectric Mechanical Reliability *(ORNL)*

Agreement 16308 – Thermoelectrics Materials by Design, Computational Theory and Structure

_____

***No report this period.**

Agreement 19201: Non-Rare Earth Magnetic Materials

Michael A. McGuire, Nirmal J. Ghimire, David J. Singh
Oak Ridge National Laboratory

Objective/Scope

We will examine rare-earth-free chemical systems which hold promise for the discovery of new high-temperature ferromagnets with the large magnetic moments and strong anisotropies required for technologically useful permanent magnet materials. This research will focus on the development of new rare-earth free permanent magnet materials. Understudied chemical systems which are likely to contain materials with properties required for useful ferromagnets (large moments, high Curie temperatures, strong magnetic anisotropy) will be synthesized and characterized. First principle calculations will be performed to aid in the identification of promising target materials and to guide chemical tuning of magnetic properties through element substitutions and alloying. The focus will be on materials based on elements, such as Mn, Fe, Co and Cr, suitable for application in vehicles.

The primary challenge in this work is to obtain high magnetic anisotropy without rare-earth elements, while maintaining high saturation magnetization. The two main sources of anisotropy are magneto-crystalline anisotropy and shape anisotropy. Magneto-crystalline anisotropy is an intrinsic property determined by energy required to rotate a magnetic moment relative to the crystal lattice. Shape anisotropy is an extrinsic property related to the domain structure of individual crystallites. We are targeting intermetallic compounds with large magneto-crystalline anisotropy, which could then be further enhanced by materials processing to optimize magnetic domain configurations. To obtain anisotropic magnetic properties, heavy transition metal elements will be incorporated instead of rare earths.

Technical Highlights

Continuing experimental investigation of Hf_2Co_{11} based alloys is improving our understanding and control over this complex hard ferromagnet. We have recently produced amorphous material by melt-spinning. Powder x-ray diffraction indicates that the crystallinity of these ribbons is significantly reduced relative to previous samples. As expected the amorphous alloy is a very soft ferromagnet with a remanent magnetization near zero and very flat M-H curve at higher fields (Figure 1, red data). Annealing experiments have resulted in partially crystallized material with strongly changed magnetic behavior (Figure 1, black data). The results are similar to those previously observed for better crystallized melt-spun materials (Figure 1, blue curve). We are continuing to study the effects of annealing time and temperature on the magnetic properties. We expect a technical report summarizing our work on these alloys to be complete in mid FY2012.

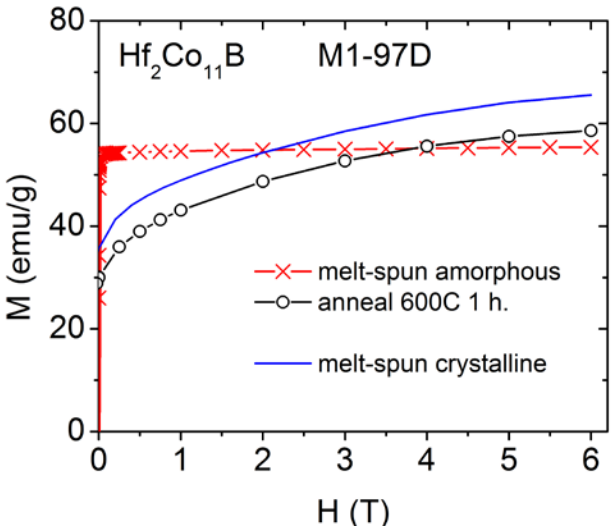

Figure 1. Magnetization curves for ribbons of compositions $Hf_2Co_{11}B$. The blue line shows results from ribbons which were found to be crystalline after melt-spinning. The red data is from ribbons which were amorphous after melt-spinning. The black data show the effects of annealing the amorphous ribbons at 600C for one hour, which resulted in increased crystallinity and properties more similar to the blue data.

In this quarter we completed our investigation of $ThMn_{12}$ type aluminides. A report on the magnetic and crystallographic properties of $ZrFe_5Al_7$, $ZrFe_{5.5}Al_{6.5}$, $ZrFe_6Al_6$, $HfFe_5Al_7$, $HfFe_{5.5}Al_{6.5}$, and $HfFe_6Al_6$ has been compiled and submitted for publication in the scientific literature. Our findings, some of which were included in our FY2011 Annual Report, are summarized here.

Figure 2 shows the magnetic behavior of samples of these materials synthesized by arc-melting and annealing. Curie temperatures range from 170 – 270 K and decrease with increasing iron content. The non-monotonic behavior of the magnetization below the Curie temperatures suggest complex magnetic interactions. Electronic structure calculations were performed to help understand these observations. The calculations indicate small magnetic moments on Zr and Hf of about 0.1 Bohr magneton. Although small, these moments could increase the magnetic anisotropy, especially for the heavier Hf. Examination of multiple magnetic structures for materials with higher Fe content indicated that there is an effective antiferromagnetic coupling between irons on the Fe1 site. Crystallographic studies showed that this site, Fe1, is the site whose occupancy is increased as the iron content is increased. Together, these results explain the three observed effects on the magnetic properties of increasing iron content: (1) the Curie temperature is decreased, (2) the saturation moment is decreased, (3) the temperature dependence of the magnetization below the Curie temperature develops a more complex, non-monotonic behavior.

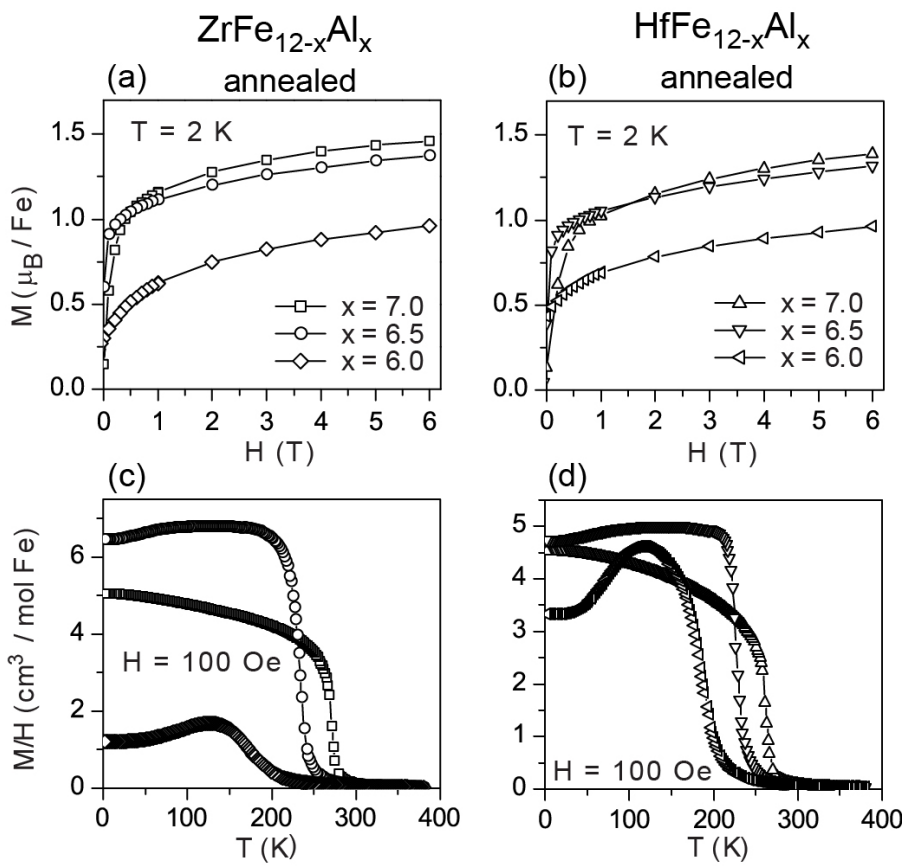

Figure 2. Magnetic properties of $ZrFe_5Al_7$, $ZrFe_{5.5}Al_{6.5}$, $ZrFe_6Al_6$, $HfFe_5Al_7$, $HfFe_{5.5}Al_{6.5}$, and $HfFe_6Al_6$. The iron content is observed to strongly affect the Curie temperature, the saturation magnetization, and the temperature dependence of the magnetization at low temperatures. First principles calculations help explain these behaviors.

<u>Status of FY 2012 Milestones</u>

Work in this Quarter involved continuation of work on Hf_2Co_{11} and completion of our study of $ThMn_{12}$-type aluminides begun in FY2011. Details regarding specific FY2012 milestones are listed below.

(1) Determine usefulness of metal flux synthesis technique for producing crystals of new ternary phosphides with transition metal concentrations approaching and exceeding 70 %, anisotropic structures, and Curie temperatures in excess of 300 °C. Results will be summarized in a report and, if appropriate, a manuscript for publication in the scientific literature. (09/2012)

Ongoing refinement of flux compositions and synthetic strategies. Crystals of particularly interesting compositions in the Hf-Fe-P system are being pursued.

(2) Develop capabilities to produce sub-nitrides using flowing ammonia gas, and examine effects of mild nitriding conditions on magnetic intermetallic compounds, with the aim of enhancing Curie temperature to values above 300 °C and increasing their

magnetic anisotropy, a requirement to produce energy products competitive with RE magnets (~ 30 MG Oe). Results will be summarized in a report and, if appropriate, a manuscript for publication in the scientific literature. (**09/2012**)

Coordination of preliminary experiments using existing facilities at ORNL are underway.

Communications/Visits/Travel
None to report.

Problems Encountered
None to report.

Publications/Presentations/Awards
Technical report entitled "Ferromagnetism in $ZrFe_{12-x}Al_x$ and $HfFe_{12-x}Al_x$ (x = 6.0, 6.5, 7.0)" submitted to *Journal of Applied Physics*.

References
None to report.

Agreement 23278: Low-Cost Direct Bonded Aluminum (DBA) Substrates

H. -T. Lin, A. A. Wereszczak, and Shirley Waters
Oak Ridge National Laboratory

Objective/Scope

This project seeks to develop low-cost, high quality, and thermomechanically robust direct-bonded aluminum (DBA) substrates. Low-cost DBA substrates will lessen the cost of the inverter insulated gate bipolar transistor (IGBT) power modules while concomitantly sustaining or improving thermal management and improving thermomechanical reliability. Compared to copper and DBC substrates, aluminum has a lower elastic modulus so it imparts a lower stress on the ceramic substrate it sandwiches, and this contributes to improved mechanical reliability of the entire substrate. Wire and ribbon for bonding in power electronic modules tends to be aluminum, so the apparent coefficient of thermal expansion of DBAs is compatible with them unlike DBCs. The use of a DBA substrate will also lessen the weight up to 50% compared to presently used DBC substrates, and this would contribute to the weight reduction goals of the inverter and converter in the APEEM program as well.

Technical Highlights

Physical properties; i.e., coefficient of thermal expansion (CTE) and thermal diffusivity of commercially available direct-bonded aluminum (DBA) and direct bonded copper (DBC) substrates were measured during this quarterly reporting period. The database will serve as a benchmark and also an input for residual stress and reliability modeling. Note the measured CTE and thermal diffusivity values would be a composite value combined contributions from each constituent (metals and ceramics) and also interface. Figure 1 shows the typical percent of elongation versus temperature curve of DBC substrates with Al_2O_3 and AlN substrate. Both substrates have the copper sheets that are cladded on both sides of Al_2O_3 and AlN substrate, which serve as an insulator. Each plot consists of two curves; i.e., first run and 2nd repeated run. It was noted that there was a large hysteresis loop for both DBC during the first run. However, the extent of hysteresis apparently decreased during the 2nd (repeated) run using the same sample. The DBC with AlN exhibited a larger hysteresis loop than that obtained for the DBC with Al_2O_3, probably due to the larger CTE mismatch existed in the Cu (16.5×10^{-6}/°C) - AlN (4.5×10^{-6}/°C) system as compared to Cu (16.5×10^{-6}/°C) - Al_2O_3 (8.2×10^{-6}/°C) system. The apparent decrease in the hysteresis loop in the repeated run would most likely result from the annealing effect during the first run that released the some of the residual thermal stress after the manufacturing process at temperature. The CTE values of these DBC substrates were then obtained from the 2nd repeated run. On the other hand, the thermal expansion curves of DBC and DBA both with AlN are shown in Fig. 2. As for both runs it is interesting to see that there is no apparent difference between these two substrates. It should be noted that Al has a lower Young's modulus (and also yield strength) than the Cu, which might have an impact to the extent of hysteresis loop even the Al-AlN system has a large CTE mismatch than the Cu-AlN system.

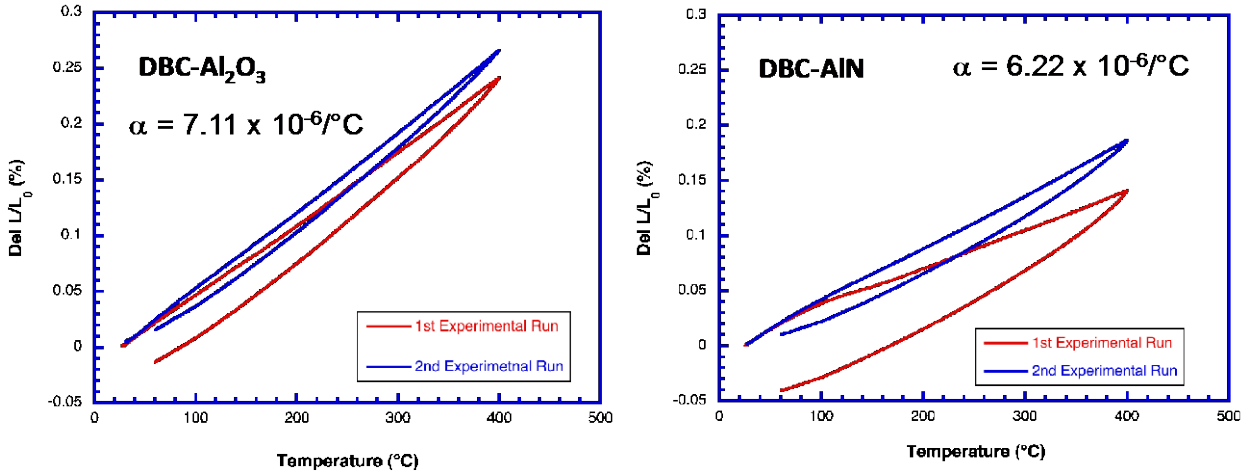

Figure 1. Percent of elongation versus temperature of DBC substrate with Al_2O_3 (LHS) and AlN (RHS) substrate.

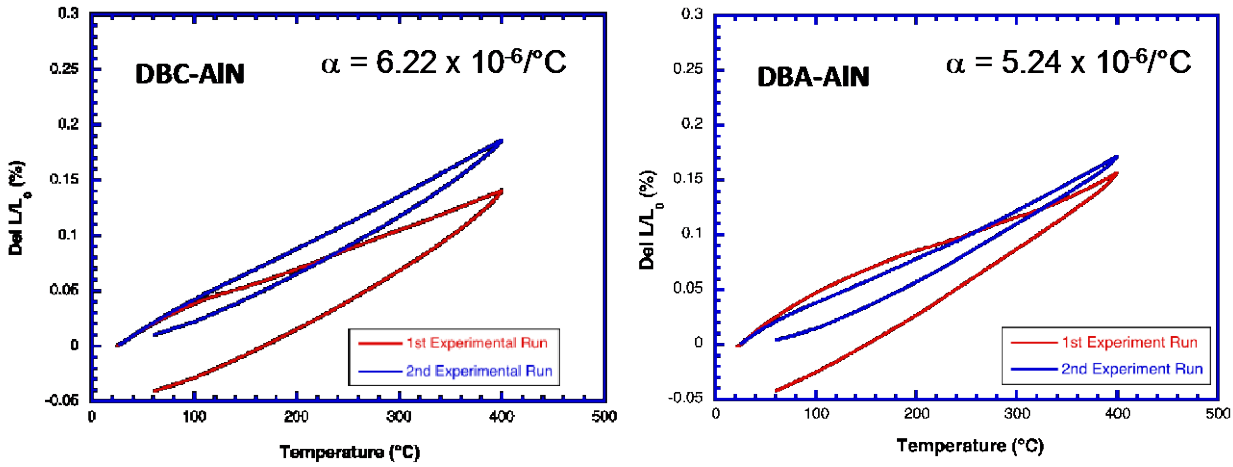

Figure 2. Percent of elongation versus temperature of DBC (LHS) and DBA (RHS) substrate with AlN substrate.

Figure 3 shows the thermal diffusivity of commercially available DBC and DBA substrates. The thermal property of these electronic substrates plays a key role to dissipate the heat that generate from the power electronic component during the operation. The capability of heat dissipation would influence the long-term reliability and life time of the system. It is naturally to anticipate that the DBC substrate with AlN exhibits the highest thermal diffusivity among the three samples (Fig. 3a). Results also showed the DBC with Si_3N_4 exhibited a 2-times higher thermal diffusivity value than the one with Al_2O_3. It is worth to note that the Si_3N_4 has much better mechanical performance than both AlN and Al_2O_3 under the stress and thermal conditions. Thus, there is an increase in use of substrate with Si_3N_4 ceramic in high power and high temperature devices because of its much improved mechanical performance and

reliability. Figure 3b compares the thermal diffusivity between DBC and DBA. The DBA substrate was manufactured with AlN ceramic. It is interesting to note that the thermal property of DBA is comparable to the DBC with AlN. On the other hand, minor difference in thermal property was observed in DBA substrates inquired from two different sources (Fig. 3c). The difference in thermal property could result from the variations in AlN purity (especially oxygen content) and interfacial microstructure and chemistry.

Status of FY 2012 Milestones

(1) Complete characterization of microstructure, and physical (coefficient of thermal expansion and thermal conductivity) and mechanical strength of commercially available DBA substrates up to 200°C. (09/2012) – On schedule.

(2) Complete fabrication of DBA substrates manufactured via new ORNL processing method and compare thermal cycling response between –40°C and +150°C in air against that of commercial DBA substrates. (09/2012) – On schedule.

Communications/Visits/Travel

- Several discussions have occurred with ORNL/NTRC, USCAR EETT, General Motors, and NREL staff members about the research and benchmarking plans for this project.

Problems Encountered

The vacuum pump system did not function properly and thus a proper vacuum could not be achieved in the furnace, which caused minor delay in the processing of DBA substrates.

Publications/Presentations/Awards

Poster on this project was presented at DOE Advanced Power Electronics and Electric Motors R&D FY12 Kickoff Meeting, Nov. 3, 2011

References

None.

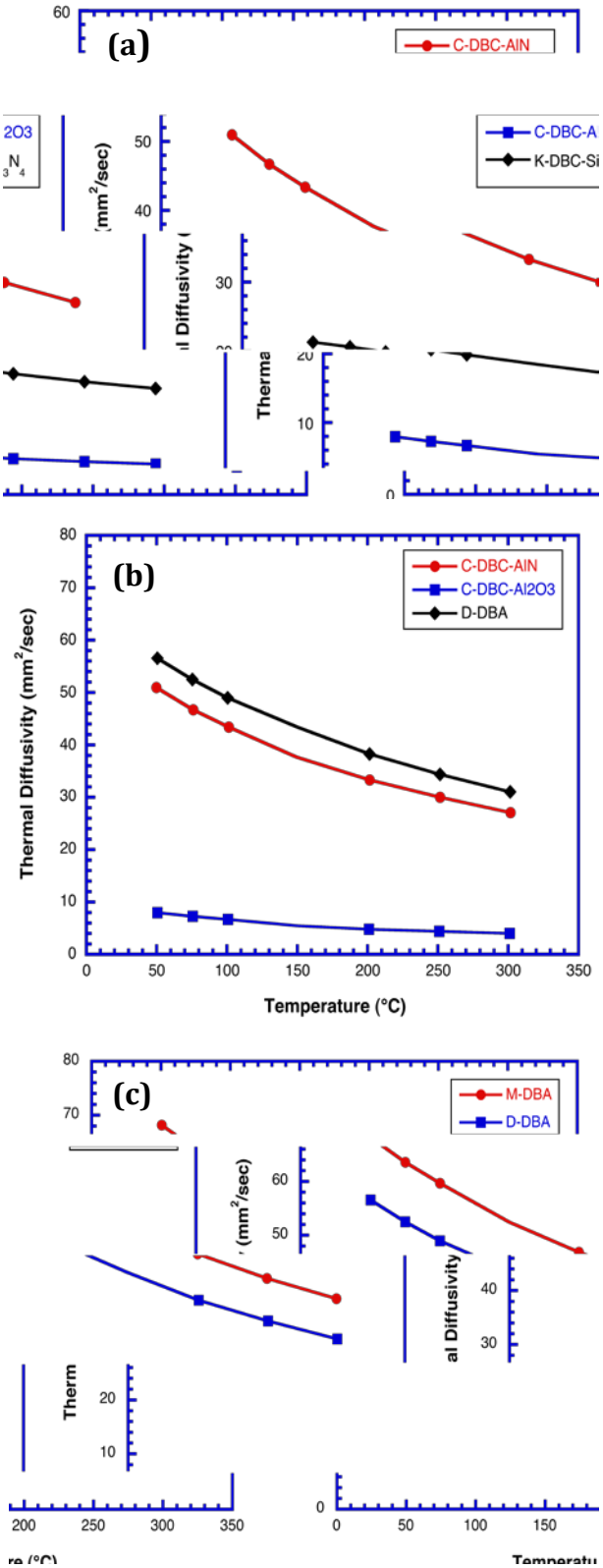

Figure 3. Thermal diffusivity versus temperature of commercially available DBC and DBA substrates.

Agreement 23279: Improved Organics for Power Electronics and Electric Motors

A. A. Wereszczak, H. Wang, and M. K. Ferber
Oak Ridge National Laboratory

Objective/Scope

Identify lower-cost and better-performing organic compounds for dielectric and thermal management applications in power electronics and electric motors. Candidate and new organic compounds (e.g., epoxy molded compounds or EMCs) will be characterized and developed to promote low-cost fabrication, volume reduction, mechanically resilience, and improved and alternative thermal management exploitation. They include compounds presently used in dielectrics in power electronic devices, potting compounds used with capacitors, and pottings used in motors. For dielectrics, improved performance represents a higher-temperature capability and the sustainment of dielectric and gel-like mechanical damping properties under thermal cycling and vibratory conditions. For potting compounds used with capacitors or motors, interest exists to identify alternatives that have higher thermal conductivity (or that enhance the thermal conductivity of existing compounds) or that benefit structural or damping performance without compromising thermal performance.

Technical Highlights

Thermal diffusivity tests were completed on recently processed EMCs with high thermal conductivity filler. Consideration of high thermal conductivity fillers is ongoing as is the analysis of a desirable particle size distribution. Discussions are underway with a filler supplier about powder coatings that will promote adherent bonding with the matrix phase.

Status of FY 2012 Milestones

Model, design, and fabricate filler-containing-EMC having 10x thermal conductivity increase over monolithic epoxy. [Sep12] *On schedule.*

Communications/Visits/Travel

None.

Problems Encountered

None.

Publications/Presentations/Awards

Poster entitled "Improved Organics for Power Electronics and Electric Motors" presented at DOE VTP PEEM R&D FY12 Kickoff Meeting, ORNL, November 3, 2011.

References

None.

Agreement 19202 – Titanium Friction and Wear
(Surface Engineering of Bearing Components)

Peter Blau and Dinesh Bansal
Oak Ridge National Laboratory

Objective/Scope

The energy efficiency and durability of internal combustion engines (ICEs), whether fueled by conventional or alternative fuels, benefit from the use of lightweight materials. Examples include polymer composites and alloys of aluminum, magnesium, and titanium. While such materials offer attractive efficiency gains, their use also presents technical and economic challenges. One class of ICE applications involves tribological aspects: that is, those which concern friction, wear, and lubrication. Studies in the United States, Japan, and the United Kingdom have shown that mechanical losses comprise about fifteen percent of the energy dissipation from fuel in a typical ICE, and that of those, energy losses by friction comprise about eighty percent. The two major subsystems, in terms of engine frictional losses, are the piston ring/cylinder interface and the crankshaft bearings, including those on the connecting rods. Past research at ORNL has focused on the piston ring/cylinder interface. The current project which began in FY 2010 not only addresses the connecting rod bearings, but it also demonstrates how surface engineering and coating technologies that could benefit other friction- and wear-critical applications as well.

The objective of this project is to *enable the use of strong, lightweight titanium (Ti) alloys for wear and friction-sensitive engine components like connecting rods (CRs) and crankshafts.* The goal is to identify the most promising surface engineering methods, whether commercialized or experimental, to reduce friction and wear of Ti alloys under engine-like conditions. This work compliments recent developments in Ti processing technology that is aimed at reducing raw materials cost. It utilizes the experience of ORNL tribology staff to effect changes in surface-critical properties via a variety of potential treatments and combinations of treatments. The phases of this three-year effort are: 1) *Friction and wear screening* of multiple surface treatments and coatings for titanium using simple coupon tests to down-select leading performers, 2) *Design and construction of a computer-controlled, variable load bearing tester* (VLBT) to simulate the contact pressure and lubricant regime excursions experienced by connecting rod bearings, and 3) *Development of a diesel engine Ti alloy connecting rod bearing concept* based on the most promising of the surface-engineered Ti treatments.

Technical Highlights

Effects of cold-working combined with diffusion treatments shows advantages. Shot peening has been used to improve the fatigue life of titanium aerospace components by introducing beneficial compressive stresses that retard crack initiation and growth, but there has been much less work on the role of shot-peening on the friction and wear of metals. When hard balls (shot) strike a metallic surface they introduce cold work (hardness), plastic deformation, and residual stresses. Prior work in this project indicated that nitriding and oxide diffusion improve the wear resistance of titanium alloy surfaces. It was therefore of interest to study the effects of shot-peening combined with diffusion treatments like nitriding and oxygen diffusion treatments. Cold-working the surface by planishing (peen hammering) was also performed to

compare it with shot-peening. A series of reciprocating ball-on-flat friction and wear experiments under severe lubricant starved conditions [ASTM G133 (Procedure A)] were conducted using the following diffusion and workhardening surface treatments::

- Bare titanium (Ti-6Al-4V) alloy (baseline)
- Shot-peening only
- Planishing only
- Nitriding plus shot peening
- Oxygen diffusion plus shot peening

The mechanical working was performed last, because the diffusion treatments involve heating the material, which could diminish the effects of mechanical working. In every case, ball bearing steel (Type 440C stainless steel) was used as the slider material, and replicate tests were performed to examine the repeatability of the results. A more complete characterization of the materials, including hardness and surface finish data, and the effects of multiple treatments versus individual treatments is being prepared for publication.

As shown in Figure 1, except for the initial running-in period, the effects of shot peening and planishing on the friction coefficient were similar. Note that each plot superimposes the results of two separate experiments on fresh, unworn surfaces. The effect of shot-peening on top of OD, reduced the friction coefficient and led to a delayed transition from lower to higher friction (see Figure 2). Note that the frictional behavior of OD plus shot-peened surfaces was relatively repeatable, the main difference being the friction transition time of 50 s versus 70 s. While this combined effect lasted, the friction was diminished by a factor of two or better. Wear measurements are being performed and will be reported later; however, initial indications are that diffusion treatments benefit Ti alloy friction and wear more than work-hardening treatments even when combined.

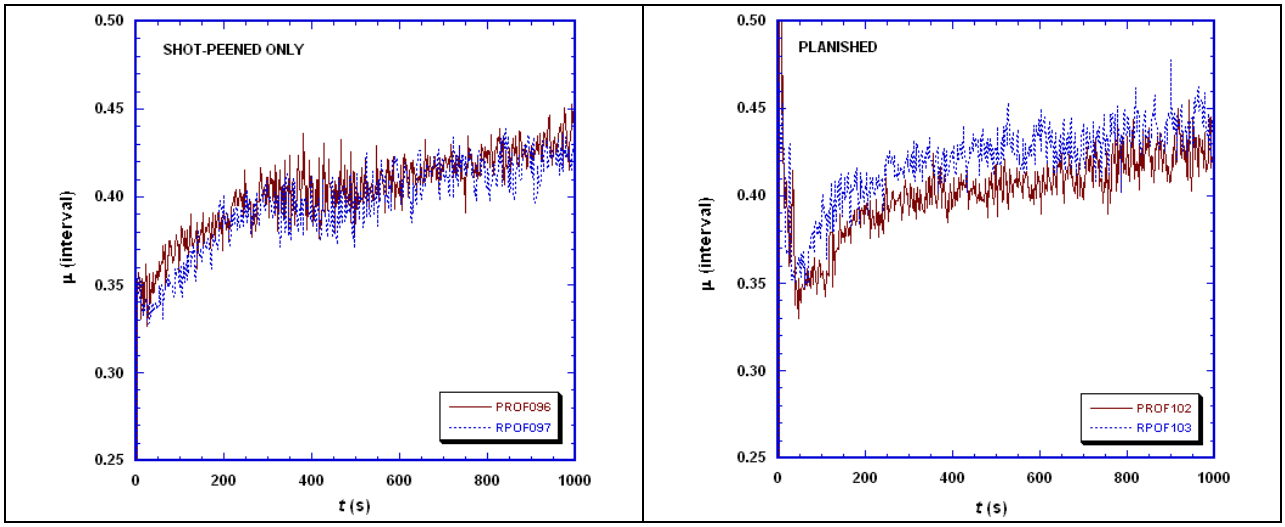

Figure 1. Effects of cold working on friction coefficient between Ti alloy and 440C steel.

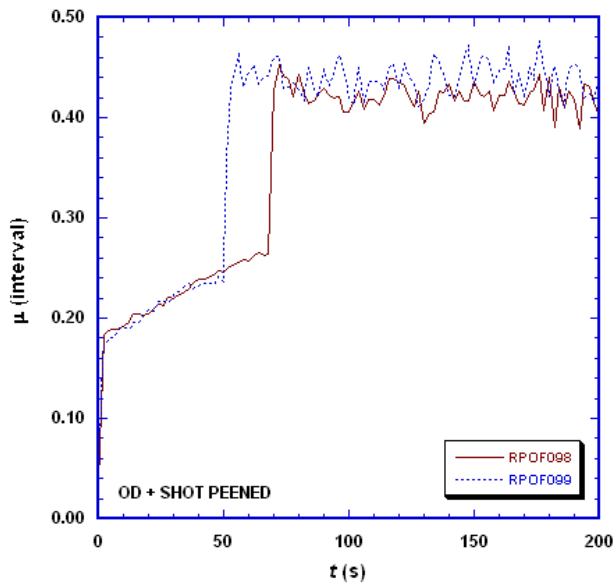

Figure 2. Effects of prior oxygen diffusion plus subsequent shot-peening on the friction coefficient under dry sliding conditions. The shapes of the $\mu - t$ curve were similar, and the friction transitions were repeatable within about 20 seconds in separate experiments.

Design and construction of variable load bearing tester (VLBT).
The design and construction of VLBT has been completed and initial baseline experiments have been performed. A close-up of the specimen fixtures was shown in Figure 1 of this project's description in the FY 2011 propulsion materials annual report. A robust, three-phase variable speed motor, controlled by a computer, drives a 25.4 mm diameter shaft to simulate the journal portion of the connecting rod large end bearing. The candidate bearing material is loaded against the shaft from underneath to contain a few drops of lubricating oil. A servo-actuator applies the load through a lever and pivot bearing arrangement. Two load cells are used: one for normal force and one for friction force.

A program in LabVIEW™ was created to control the test rig while simultaneously acquiring normal force, friction force and speed data. The test rig can apply a predetermined variable load profile which is repeated for the test duration. Thus the test rig provides a unique capability for studying wear and friction of bearing materials under transient (spectrum) loading.

The effects of constant load versus varying load on friction and wear under lubricated conditions were demonstrated using the VLBT. Two tests were run using an AISI 8620 steel shaft and a Ti-6Al-4V alloy flat specimen. The sliding speed was 1 m/s (754 rpm) to produce boundary lubrication conditions (Cummins Blue™ 15W40 diesel oil). One test was run with a variable load profile and the other one under constant load. In the first test, the loads were varied as follows: 9.8–37.5–65.3– 94.5–94.5–65.3–37.5–9.8 N, holding each step constant for 15 s. This load cycle was then repeated over the test duration of 1100 s. In the second test, a constant load of 51.7 N, which was equivalent to the average load during one complete load cycle of Test 1, was applied for the entire duration. Figure 3(a) shows the variation in the normal force and the coefficient of friction (COF) during Test 1 with variable loading, while

Figure 3(b) presents the similar scenario for Test 2 with a constant load. Under varying loads the average COF for a given load increases as the test progresses, in contrast to that for the constant load test where the COF shows a steady value of around 0.3 after the initial run-in period.

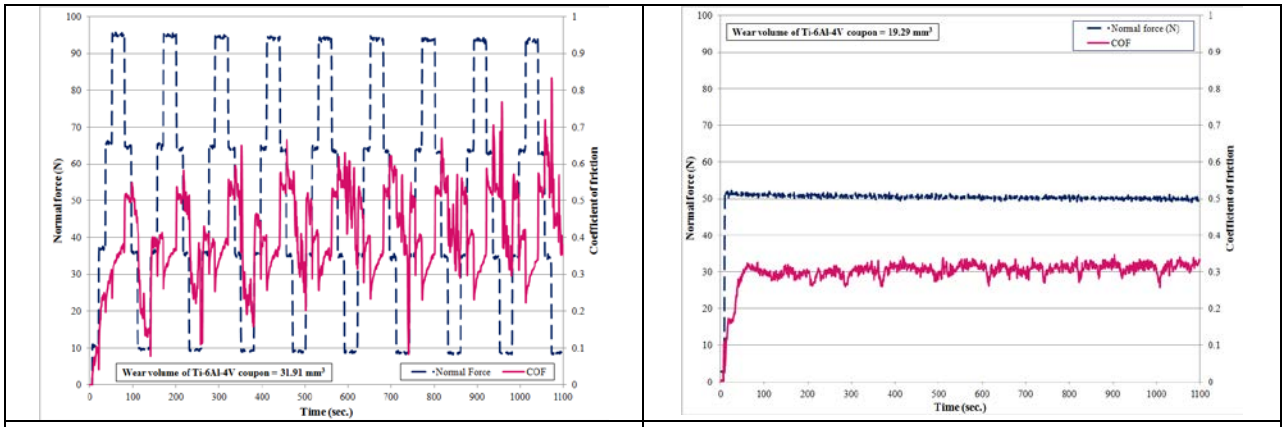

(a) (b)

Figure 3. Comparison of load profiles and friction coefficients for a variable load test (a) and constant load test (b). The sliding speed, duration, and average normal force was the same for both tests, but the friction and wear behavior was quite different. (Vertical scales are equal on both figures.)

Table 1 compares the wear volumes and the frictional work done. Note that for the variable load test, the frictional work done is only for the last of nine step-loading cycles. Friction work, as considered here, is the product of the friction force and the distance slid. Thus, the total frictional work for a step loaded test sums the products of friction force and distance slid for each step in the test. It is seen that work done in the last full load cycle of Test 1 (variable load) is about 32% higher than the work done for all of Test 2 at constant load. Also, the wear volume of the Ti64 coupon for Test 1 (from measurements of the scar depth profile) is about 65% greater than that for the constant load test.

Table 1. Comparison of Wear Volume and Frictional Work per Cycle for Diesel Oil Lubricated Tests of 8620 Steel Against Ti-6Al-4V

	Wear volume of Ti64 coupon (mm^3)	Frictional work done per cycle (Joule)
(1) Variable load test	31.91	2376.6
(2) Constant load test	19.29	1804.1

The most transformative finding of these initial experiments on the VLBT was the importance of conducting tribo-tests under varying load conditions rather than constant load in order to more realistically simulate components like large-end bearings that experience variable loads during operation. Varying load produces interfacial transients during which the lubricant film thickness, and hence the degree of solid-solid contact, varies. At times when the lubricating film is thinnest, the wear process is exaggerated. Adopting such a load-spectrum approach to screening boundary and mixed-film lubricated engine component materials is well-advised, and will be used extensively in this project.

Future Plans.

- To determine optimum test conditions for evaluating five different surface treatments on variable load bearing tester (VLBT)

- Conduct optimization study on other down-selected surface treatments for use in the concept design for a connecting rod large-end bearing.

Status of Milestones

1) Complete tests of candidate coatings and multiple surface treatments using the variable-load bearing test system (VLBT)**. (09/11)** *Postponed until 6/2012 to make improvements in the VLBT fixtures, electronic motor controls, and data acquisition program.*

2) Complete analysis of VLBT test surfaces and prepare a final report summarizing the work on this effort that culminates in a design concept for Ti-alloy connecting rods with integral bearing surfaces. (09/12)

Communications/Visits/Travel

None this quarter.

Problems Encountered

The VLBT was not performing as expected based upon the original design concept, so changes had to be made in both mechanical and electronic controls systems. This delayed the start of screening tests under variable-load conditions, but the system is now operational.

References

None

Publications and Presentations

None this quarter.

Agreement 23284: Friction Reduction Through Surface Modification

Peter J. Blau and Stephen M. Hsu*
Oak Ridge National Laboratory
***George Washington University, Ashburn, VA**

Objective/Scope

The primary objective of this two-year effort is to improve the fuel efficiency of diesel-powered vehicles by reducing the friction of contacting surfaces by employing specific patterns of micro-scale features. These features function in two ways: (1) to increase the lubricant film thickness, which separates bearing surfaces, and (2) by trapping harmful wear debris in depressions below the contact surface. One bearing surface of particular interest is that between the piston ring and cylinder liner, although other frictional surfaces in engines, like those of bucket lifters and cam lobes are also of interest.

The scope of this effort includes the preparation and testing of textured bearings by various surface engineering methods. During FY 2011, ORNL prepared indentation-textured surfaces on bearing materials, and investigated the effects of on wear and friction as a function of sliding time. Changes in the morphology of the surfaces during the running-in stages were correlated with the friction coefficient versus time sliding history. Understanding the running-in period is key to separating the contributions of as-finished surface roughness, wear-in, and lubricant conditioning as the bearing system approaches its longer-term, steady-state condition. A subcontract with George Washington University complements in-house efforts by developing and demonstrating a new masking technology to enable the surface patterning of curved surfaces like those on piston rings and cylinder bores.

Technical Highlights

Survey of Prior Research on Texturing. A review of previous research on the application of surface patterns to control friction was completed and is under internal review prior to release as an ORNL technical report. It contains an appendix that lists bearing-related applications to which textures have been applied as well as the methods used to produce them. The pros and cons of texturing are also discussed. The report's title is: "Use of Textured Surfaces to Mitigate Sliding Friction and Wear of Lubricated and Non-Lubricated Contacts."

Indentation Array Texturing. As mentioned in the annual report and the previous quarterly, experiments were conducted to investigate the effects of indentation array texturing (ITx) on friction of bearing bronze (CDA 932) and titanium alloy (Ti-6Al-4V). The purpose of these experiments was to understand the effects of material type on the degree to which texturing can ameliorate scuffing-prone material combinations when sliding under boundary lubrication. Using an automated microindentation tester, a square array of 3600 Vickers microindentation hardness indentations was placed on polished flat surfaces with a lateral spacing of 150 µm along the rows and 75 µm between rows. Reciprocating sliding tests were conducted using a ball-on-flat configuration (52100 steel balls) and under boundary lubrication (fresh diesel engine

oil). Some of the steel slider balls were pre-conditioned by on abrasive paper to produce a flat spot. In other cases, spherical sliders were used. Results indicated that friction was reduced more by polishing the slider tips than by applying textures. Furthermore, texturing was more effective on the bronze than on the titanium. The reason can easily be seen in Figure 1 where adhesive wear obliterated the titanium texture array but left most of the bronze array intact. The conclusions to be drawn were: (a) For counterformal contacts, using a smooth flat surface has a greater benefit on friction reduction in the boundary lubrication regime than does ITx, and (b) texturing worked better on leaded bronze because, despite its lower hardness, it is more wear resistant against Type 52100 steel than Ti-6Al-4V.

Progress at George Washington University (subcontract). During the past quarter, GWU developed several tests. The first is a ring-on-liner test method using a commercial reciprocating sliding test apparatus (Plint Model TE 77, UK). The test allows systematic surface texture evaluation under the three dominant lubrication regimes: 1) boundary lubrication; 2) elastohydrodynamic lubrication; and 3) hydrodynamic lubrication. In addition, the overall effectiveness of texturing was measured for a simulated stroke using an original equipment manufacturer's (OEM) proprietary test procedure. Together, these two methods will be used to optimize various surface textures according to their dominant lubrication mechanism and the global frictional resistance. This will enhance the probability of success when designing the surface of a whole piston ring for engine testing by the OEM.

Cam-follower test procedure development. Progress was also made in developing a third test procedure to evaluate the effects of texturing for the cam roller follower application. A commercial block-on-ring (Falex Corp., Illinois USA) test rig was used to simulate the cam-follower contact (see Figure 2). The block specimen rests against a rotating ring specimen under a fixed load. The test chamber is filled with lubricant to a level just above the center of the shaft that holds the ring specimen. Ring specimen rotation brings the lubricant into the contact zone. The rings are Falex standard test specimens (SAE4620 steel, hardness HRC 58-63) of 35 mm outside diameter. The rms roughness of the ring surface is 25 µm. The block specimens are Falex standard flat test blocks of tool steel (hardness HRC 58-63). The thickness of the block is 6.35 mm. To avoid the rapid contact stress changes during the wear-in process, the face of the slider block was pre-worn to a scar width of 0.5mm ± 0.02 mm using a white oil without anti-wear additives. The pre-formed scar was then polished before the texture was finally applied. A combination of rotational speeds and applied loads was used to produce mixed, elasto-hydrodynamic and hydrodynamic lubrication regimes. Initial tests at various conditions were conducted to establish their effects on friction under baseline, non-textured conditions.

Based on GWU's knowledge of texture design and extensive laboratory bench testing, two types of simple texture designs were selected to compare with baseline results: one with elliptical dimples and the other with circular dimples. First, a soft mask and photolithography technique was used. This was followed by electro-chemical etching to fabricate the textures on the pre-worn block specimens. The applied load was in the range of 20 - 80 lbs, and the speed range was 100 - 600 rpm. Consequently. the apparent contact stress was in the range of 30 – 120 MPa, and the sliding speed was in

the range of 0.18 – 1.1 m/s. White oil (ISO 32 grade equivalent) with 2% Tricresylphosphate and 1% antioxidant was used as the lubricant. This simple formulation prevented rapid degradation of lubricant without affecting its friction characteristics. For each applied load, the test procedure starts with 600 rpm, then steps down to 100 rpm with a decrement of 100 rpm. The test runs 2 minutes for each speed step while friction force is recorded. The procedure is repeated for other loads ranging from 20 to 80 lbs and with 10-lb increments.

Friction data for speeds of 100 rpm, 400 rpm and 600 rpm can be compared in Figure 3. Similarly to the approach used to model sliding bearings, a dimensionless parameter $\eta V(L/W)$ was used to analyze the data. Symbols are defined as follows: η is the viscosity of the lubricant, [Pa•s]; V is the linear speed of ring specimen, [m/s]; L is the width of the block specimen, [m]; W is the applied load, [N]. The average friction force at each load/speed step was used to calculate the friction coefficient, then the measured friction coefficient was plotted against the dimensionless parameter $\eta V(L/W)$ which reflects both test parameters and lubricant properties.

As expected, the texture design using circular dimples has a higher friction coefficient than that of the baseline. This confirms both GWU's past experience and findings from the literature [1-3]. However, the texture design with elliptical dimples reduced friction at all speeds and applied loads. Compared to the baseline results, the overall friction reduction of an ellipse-shaped texture design is in the range of 12-20%. Significantly, up to 85% in friction reduction was observed for the ellipse texture designs under low-load, high-speed conditions.

Status of FY 2012 Milestones

1) (GWU subcontract) Submit report on the Cameron-Plint test procedure and the associated data for friction reduction under various conditions (12/31/2011). *Status: completed on schedule*.

2) (GWU subcontract) Develop a test procedure using an Atomic Force Microscope to measure the influence of nanoclay particles on the global mechanical properties of the clay infiltrated nanocomposites. Submit report containing an AFM test procedure in an ASTM standard format (1/31/ 2012). *Status: on schedule for on-time completion*.

3) (ORNL) Conduct lubricated friction tests using ASTM G181, and curved specimens with patterns found to offer the most promise for friction reduction and present a report on the results (6/30/12). *Status: work in progress*

4) (ORNL) Working with a U.S. diesel engine manufacturer and George Washington University, develop a guideline report for applying textured surfaces to pistons and other promising components to affect fuel savings (9/30/12). *Status: work in progress*.

Communications/Visits/Travel

Prof. Stephen Hsu, George Washington University, visited ORNL on November 9, 2011, to discuss progress on his subcontract work. He presented a talk on scientific approaches to optimizing surface textures for friction reduction and discussed his interactions with Cummins Engine Company. After a tour of the ORNL tribology laboratory, we discussed plans to collaborate on testing piston rings that would be provided by ORNL and textured at GWU.

Problems Encountered

None.

Publications/Presentations/Awards

P. J. Blau (2012) "Use of Textured Surfaces to Mitigate Sliding Friction and Wear of Lubricated and Non-Lubricated Contacts – An annotated literature review," ORNL Technical Report, 30 pp. – currently under review for publication.

References

[1] Yang, P., Cui, J., Kaneta, M., Nishikawa, H., "Influence of surface bump or grove on the lubricating performance and dimple phenomena in simple sliding point EHL contacts," ASME Trans., 126, 466-472, 2004.

[2] Ronen, A., Etsion, I., Kligerman, Y.,"Friction-reducing surface texturing in reciprocating automotive componenets," Tribology Trans., 44, 3, 359-366, 2001.

[3] Wang, Q. and Zhu, D., "Virtual Texturing: Modeling the Performance of Lubricated Contacts of Engineered Surfaces," Journal of Tribology, 127, 722-728, 2005.

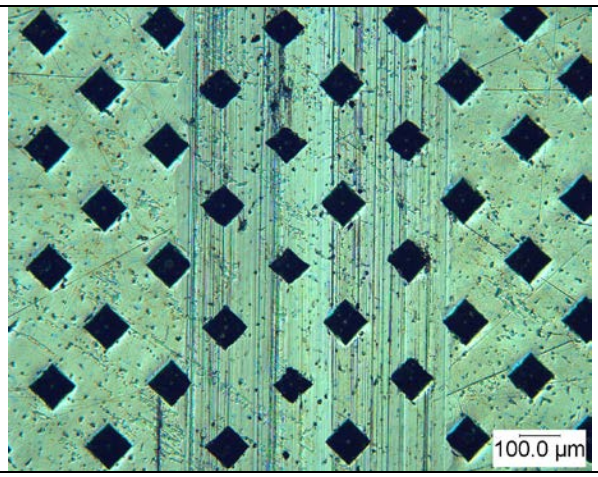

Bronze wear track showing surviving impressions in the worn region (vertical abrasion marks)

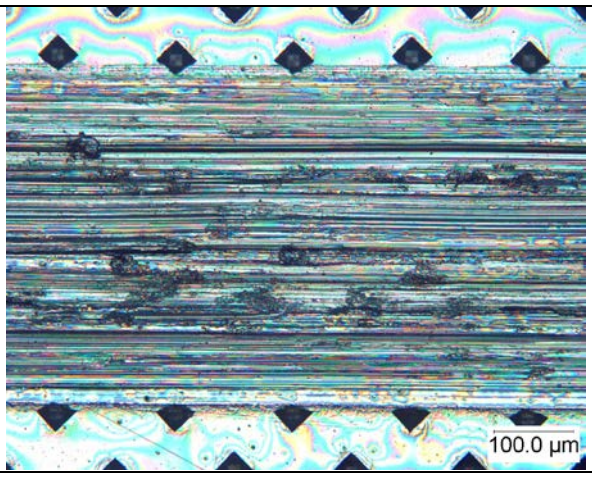

Titanium wear track with an obliterated texture (color fringes are from residual lubricant)

Figure 1. Wear tracks on ITx surfaces of two alloys: CDA 932 bronze (left) and Ti-6Al-4V (right).

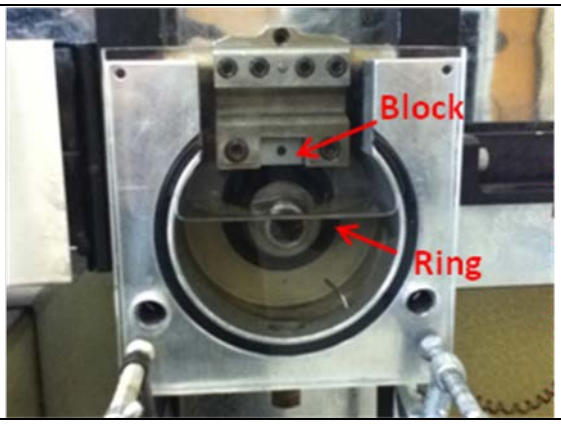

Figure 2. Block-on-ring test configuration in its lubricant retention chamber.

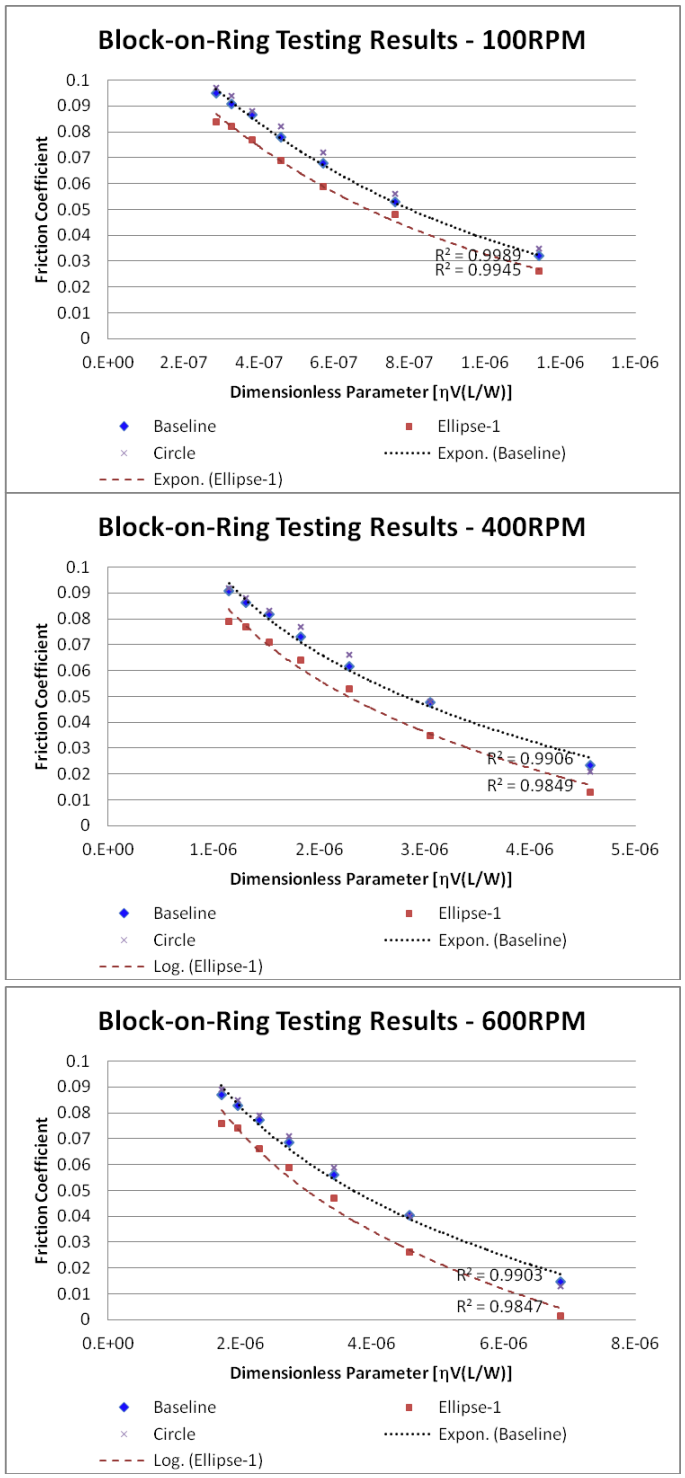

Figure 3. Friction coefficient comparison of surface textured metal specimens at various speeds (a non-textured block is used as a baseline; texture contains ellipses and circles)

Agreement 11752: Materials for High Efficiency Engines

Govindarajan Muralidharan and Bruce G. Bunting
Oak Ridge National Laboratory

Objective/Scope

To identify and catalog the materials operating conditions in the HCCI engines and utilize computational design concepts to develop advanced materials for such applications.

Technical Highlights

In this quarter, work was continued on Ni-based alloys for valve applications. As reported earlier, using thermodynamic modeling, microstructure evaluation, and mechanical property evaluation, high temperature fatigue was identified as a property of critical interest in Ni-based alloy valve materials for the next generation automotive engines. In order to develop relationships between the microstructures of the alloys and their mechanical properties, high-temperature fatigue property data were obtained on all down-selected alloys as a part of the project. Using the approximate correlation between the fatigue lives obtained using the rotating beam and fully reversed fatigue testing techniques several alloys with required microstructures have been identified as candidates for high temperature valve applications.

Using the microstructures of these alloys as a guide, computational thermodynamics was used to identify additional alloys with microstructure similar to the commercial alloys with desirable properties. In contrast to the commercially available alloys with high Nickel contents (> 75%), the Ni-content in these alloys ranges from about 30 wt. % to 45 wt. % with the potential to achieve comparable properties. This implies that the alloys will be of lower cost but comparable mechanical properties.

Results from the fatigue tests on newly developed alloys HCCI-9 and HCCI-16 showed that new alloys with greater strength levels were required to perform at 870°C and stress levels of 35 Ksi. In this quarter, work continued in designing and fabricating new alloys aimed at increasing the strength levels. These alloys were vacuum arc cast into billets of size 1”x1”x3”, rolled, heat-treated, Table 1 shows the newly developed alloys and their measured yield strengths at 870°C in the aged condition.

Alloy Designation	**Yield Strength at 870°C (Ksi)**
HCCI-490-1	65.4
HCCI-490-2	68.8
HCCI-490-3	66.7
HCCI-490-4	66.6
HCCI-490-5	63.5
HCCI-490-6	62.0

Results confirm that a larger Nickel content is favorable for achieving increased yields strengths. Further effort will be required to achieve yield strengths of >75Ksi. Two alloys will be downselected and larger heats will be prepared for rotating beam fatigue testing.

Status of FY 2012 Milestones:

(1) Complete rotating beam fatigue tests on at least two new alloys at 870°C, and stress greater than 25 Ksi.(9/2012) On Track

(2) Demonstrate a lifetime of >100 million cycles to failure at a stress level greater than 25 Ksi. (9/2012) On Track

Communications/Visits/Travel

Problems Encountered

Publications/Presentations/Awards

"Effect of Microstructure Evolution on the High Temperature, High Cycle Fatigue Properties of Two Ni-Based Superalloys," G. Muralidharan, R. Battiste, E. A. Kenik, and James Bentley, Presentation made at the MS&T 2011, Columbus, OH, Oct. 16-20, 2011.

References

Agreement 13329: Design Optimization of Piezoceramic Multilayer Actuators for Heavy Duty Diesel Engine Fuel Injectors

H.-T. Lin, H. Wang, K. Zhang, F.W. Zeng, and A. A. Wereszczak,
Oak Ridge National Laboratory

R. Stafford and D. Memering
Cummins Inc.

Objective/Scope

Enable confident utilization of piezo stack actuator in fuel injectors for heavy vehicle diesel engines. The use of such actuators in diesel fuel injectors has the potential to reduce injector response time, provide greater precision and control of the fuel injection event, and increase fuel efficiency. Though piezoelectric function is the obvious primary function of lead zirconate titanate (PZT) ceramic stacks for fuel injectors, their mechanical reliability can be a performance and life limiter because PZT ceramic is intrinsically brittle, lacks high mechanical strength, and is susceptible to fatigue. However, that brittleness, relatively low strength, and fatigue susceptibility can be overcome with the use of appropriate structural ceramic probabilistic design and reliability methods.

Technical Highlights

1. Testing and Characterization of PZT Ceramics

Testing on EPCOS PZT ceramics resorted to different configuration because the stand-alone single-layer PZT was not available; particularly, 10-layer plate specimens were used.

Two sizes of 10-layer plates were used in this project. The first size was 6.8 mm × 6.8 mm × 0.76 mm. These specimens were extracted from three commercial EPCOS PZT stacks (6.8 mm x 6.8 mm x 30 mm) using chemical solution along with heating. These stacks had been tested and found dielectrically broken. The extracted specimens were tested using ball-on-ring (BoR) setup of ϕ6.35 mm Si_3N_4 ball and ϕ5.12 mm polymer ring at room temperature (RT, 22°C) in FY09. This was conducted in a custom-made indentation system under the displacement control mode with loading rate of 0.01 mm/s. A 100-lb load cell was used in tests for measuring the mechanical force. The Weibull plot of fracture stress (or strength) is given in Fig. 1(a).

The second size was 12 mm × 12 mm × 0.74 mm. The specimens were also extracted from commercial EPCOS PZT stacks (12 × 12 × 54 mm^3), but using a dedicated process carried out by Cummins, Inc. The obtained specimens were tested in this quarter reporting period using a BoR setup with ϕ6.35 mm steel ball and ϕ9.95 mm steel ring also at room temperature (RT, 22°C). A 10-lb load cell was used. The Weibull plot of strength of 10-layer specimens is given in Fig. 1(b). The size effect on the mechanical strength of such multilayer specimens is seemingly

quite apparent. The specimens with larger size had a significant decrease (~8%) in fracture strengths. These can be seen more clearly in the confidence ratio rings as demonstrated in Fig. 2.

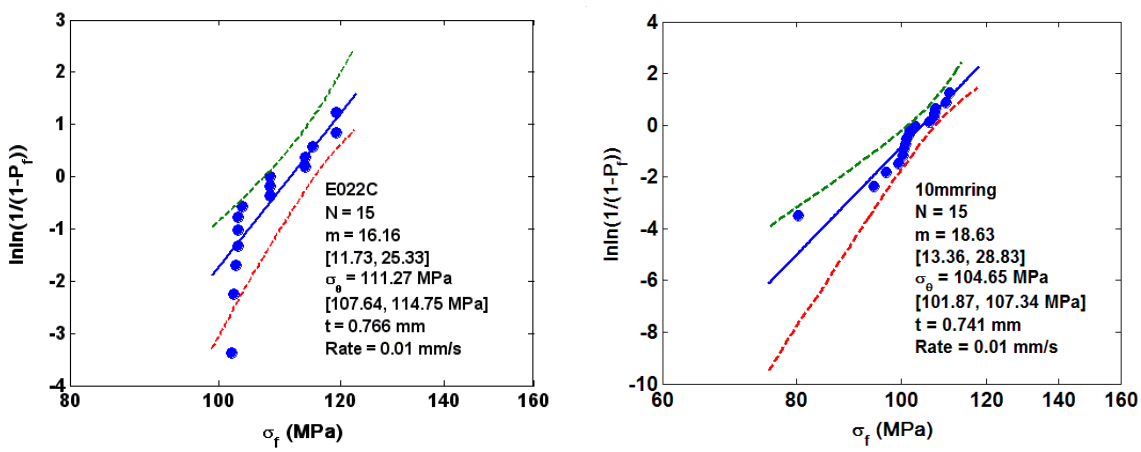

(a) (b)

Fig. 1 Weibull plot of fracture stress based on BoR test of 10-layer plate specimens with a size of (a) 6.8 × 6.8 × 0.76 mm^3, and (b) 12 × 12 × 0.76 mm^3.

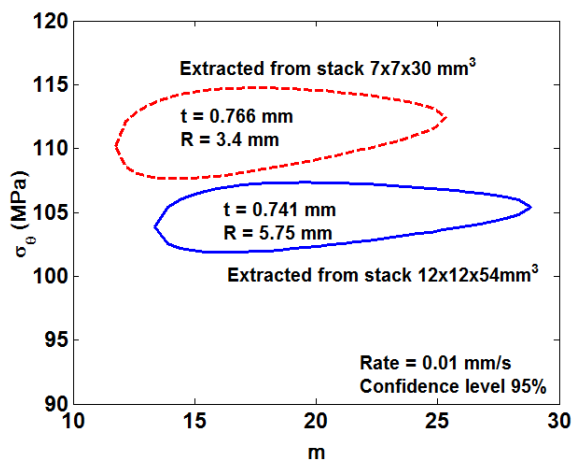

Fig. 2 Confidence ratio rings of mechanical strength of 10-layer specimens in 95% confidence level.

Scanning electron microscopy (SEM) fractographical study illustrated that failure origin (pore or agglomerate) is located in the outer PZT layer as shown in Fig. 3. Similar results were also obtained for the smaller size of 10-layer plate specimens (6.8 mm × 6.8 mm × 0.76 mm). Therefore, the experimental approach proposed here indeed characterized the strength property of PZT. This observation agrees with the relative thickness of metal electrodes to PZT layers (4 μm versus 80 μm).

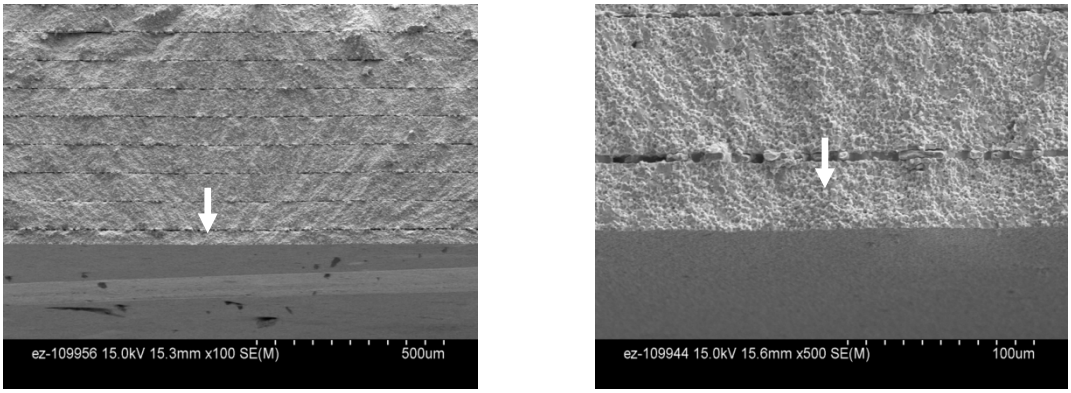

(a) (b)

Fig. 3 SEM photomicrographs of the failure origin at X100 (a) and X500 (b).

2. Testing and Characterization of PZT Stacks

Uncapsulated EPCOS stacks (12 mm × 12 mm × 54 mm, 16.15 μF, rated voltage 160 V) were screened. The stack that still has good electric resistance was selected and prepared for the cycling test. The piezo stack fatigue setup that was built for the small EPCOS stacks (6.8 mm × 6.8 mm × 30 mm) was being modified, including the transmitting rod, guiding rods, and target rods. The on-line displacement monitoring will be conducted with the help of high frequency amplifiers (410-XS-6WB, 6 kHz, Capacitec) once the components are received.

The alternative is pursued to test low-profile PZT stacks using piezodilatometer. Aged (> 3 years) 10-layer PZT plates, NOLIAC CMAP07 (5 mm × 5 mm × 2 mm, 10 nF, rated voltage 200 V) are being tested under a controlled electric loading. The piezodilatometer is currently equipped with a Trek PZD 2000A that has a current capacity of ± 400 mA at ± 2kV enabling accelerating fatigue test. The test to define the safety operation area (SOA) was conducted for such short stacks by cycling at various combinations of specified frequencies and field levels for 5 minutes. Three points corresponding to dielectric breakdown were obtained and are shown in Fig. 4. The electric cyclic fatigue is being considered and the adaptation of setup on piezodilatometer is undergoing to accommodate such size of PZT stacks.

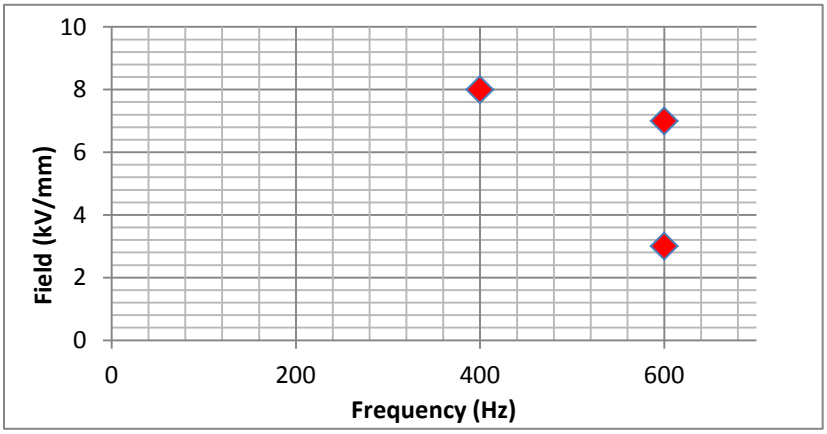

Fig. 4 Results of safety operation area for aged NOLIAC short stacks (CMAP07)

Status of FY 2012 Milestones

Measure and compare reliability of competing commercially available piezoactuators under consideration for use in diesel fuel injectors, *on schedule*.

Communications/Visits/Travel

Communications via e-mail and phone call on CRADA updates with Dr. Randy Stafford of Cummins, Inc. were routinely maintained.

Publications/Presentations/Awards

1. Wang, H., Matsunaga, T., Lin, H.-T., and Mottern, A. M., Piezoelectric and Dielectric Performance of Poled Lead Zirconate Titanate in Electric Cyclic Fatigue, Smart Materials and Structures, accepted.
2. Zhang, K., Wang, H., and Lin, H.-T., Strength Properties of Aged Poled Lead Zirconate Titanate Subjected to Electromechanical Loadings, submitted.

References

None

Agreement 17257: Materials for Advanced Turbocharger Designs

P.J. Maziasz and A. Shyam
Oak Ridge National Laboratory
and
K. Pattabiraman
Honeywell Turbo Technologies

Objective/Scope

This ORNL CRADA project with Honeywell, NFE-08-01671 (DOE/EERE/OVT Agreement 17257) began last year, and is scheduled to last for about 3 years. This CRADA project addresses the limitations of lifetime or use-temperature for the various components (casing, wheel, shaft, bearings) of both the turbine and compressor parts of the turbocharger system. As exhaust temperatures increase, to provide higher engine efficiency and lower emissions, turbocharger component temperatures also increase, so the need for more heat-resistant materials must be addressed. Requests for more detailed information on this CRADA project should be directed to Honeywell, Inc.

Highlights

Neutron-scattering experiments at ORNL to measure residual-stresses in critical locations of wheel/shaft assemblies and turbine housings were completed last quarter. Long-term creep-testing of cast CF8C-Plus austenitic stainless steel at 600°C continued this quarter, and aged specimen became available for testing this quarter. Assessments of the oxidation-resistance of CF8C-Plus steel relative to other exhaust component cast-irons and steels continued this quarter.

Technical Progress, 1st Quarter, FY2012

Background

This CRADA project began last year, and will extend for 3 years, and covers several different tasks. The first task was to assess and prioritize the various components that need or would most benefit from materials upgrades to increase temperature capability and performance, as well as durability and reliability. The next tasks examine current performance and degradation modes of wheel/shaft assemblies for turbines and compressors, housings for turbines and compressors, and bearings. These tasks may then obtain and test new materials with upgraded performance, and provide the results to Honeywell for designing advanced turbocharger systems, or for manufacturing of new prototype components for testing and evaluation.

Approach

This CRADA project began early last year. This project is comprised of six tasks, which will span the next 36 month period. Activity began with ORNL and Honeywell discussing the priority of the various turbocharger components for materials upgrades. A turbocharger system includes the hot (turbine) end, driven by exhaust gas from the engine, a cold (compressor) end to increase air pressure into the combustion changer, and a transition region that connects these two ends. The turbine and compressor wheels are connected to a common shaft, supported by bearings. For the first task, the turbine wheel-shaft assembly was chosen as the first component for consideration, with analysis focused on residual stresses near the weld-joint of the Ni-based superalloy wheel to the steel shaft, which can upset balance during service. Another task of this new CRADA project continues previous work between ORNL and Honeywell on testing of the new CF8C-Plus cast stainless steel as a significant performance upgrade for the turbine housings relative to standard SiMo or Ni-resist cast irons. This CRADA project for turbine housings covers a broad range of other high temperature properties, including creep and fatigue strength, and includes turbine housing applications for passenger vehicle gasoline engines.

Technical Progress

For Task 1, Honeywell identified neutron-scattering experiments to measure residual stresses in welded wheel/shaft assemblies as one of their highest priority items. For Task 2, these experiments were defined, and neutron scattering experiments at the HFIR Residual Stress User- Facility began last quarter. Figure 1 shows a typical Honeywell wheel/shaft assembly. Preliminary neutron-scattering experiments for diffraction analysis of the steel shaft began previously, and additional experiments on wheel/shaft assemblies with variations in processing parameters continued and were completed last quarter.

For Task 3, ORNL continued long-term creep-rupture tests at 600°C of the cast CF8C-Plus stainless steel this quarter, with one test at a higher stress rupturing after 7,300 h, and another test at a lower stress continuing beyond about 13,700 h. ORNL completed aging of as-cast CF8C-Plus tensile/creep specimens at 700 and 800°C to 2500 h last quarter, and mechanical properties testing of the aged specimens began this quarter and will continue next quarter. ORNL also completed additional longer-term creep-rupture testing at 700-850°C that will add to previous creep-rupture data on CF8C-Plus and HK30-Nb steels. Honeywell is addressing the next steps necessary to commercially produce some prototype turbocharger housing using CF8C-Plus steel for the Ford 3.5L V-6 Ecoboost engine used in light trucks. This is the next step required so that new housings can be evaluated and tested on engines.

Figure 1 – Honeywell turbocharger wheel/shaft assembly used for neutron-scattering experiments, consisting of a Ni-based superalloy turbine wheel welded to a steel shaft.

Oxidation experiments to assess the oxidation-resistance of cast CF8C-Plus relative to several cast-irons used for conventional turbochargers and exhaust system components began previously, and continued this quarter.

Communications/Visits/Travel

Periodic conference calls are held between ORNL and Honeywell Turbo Technologies, and email communications help to coordinate the work.

Status of Milestones (ORNL for DOE)

The FY2012 milestone to begin initial neutron-scattering residual-stress measurements on wheel/shaft assemblies for turbochargers (12/2011) was achieved, and the other milestones for FY2012 are on-track.

Publications/Presentations/Awards

None

Agreement 18571: Materials Issues Associated with Exhaust Gas Recirculation

M. J. Lance, C. S. Sluder, M. K. Ferber and J. M. E. Storey
Oak Ridge National Laboratory

Objective/Scope

Provide information to industry specialists about fouling deposit properties so as to enable improved models and potential design improvements to reduce fouling and its impact on the performance of EGR (exhaust gas recirculation) coolers.

Technical Highlights

The bench-flow reactor was redesigned to reduce the flow length between the furnace outlet and the heat exchanger inlet in order to increase the inlet gas temperature. The furnace is now just 2 inches away from the heat exchanger which allows us to achieve inlet gas temperatures of 450°C. Figure 1 shows the redesigned system and the location of the thermocouples which allow us to measure the effectiveness of the heat exchanger. A LabView Virtual Instrument was created to read these temperatures, control the furnace, and control the setpoint of the mass flow controllers.

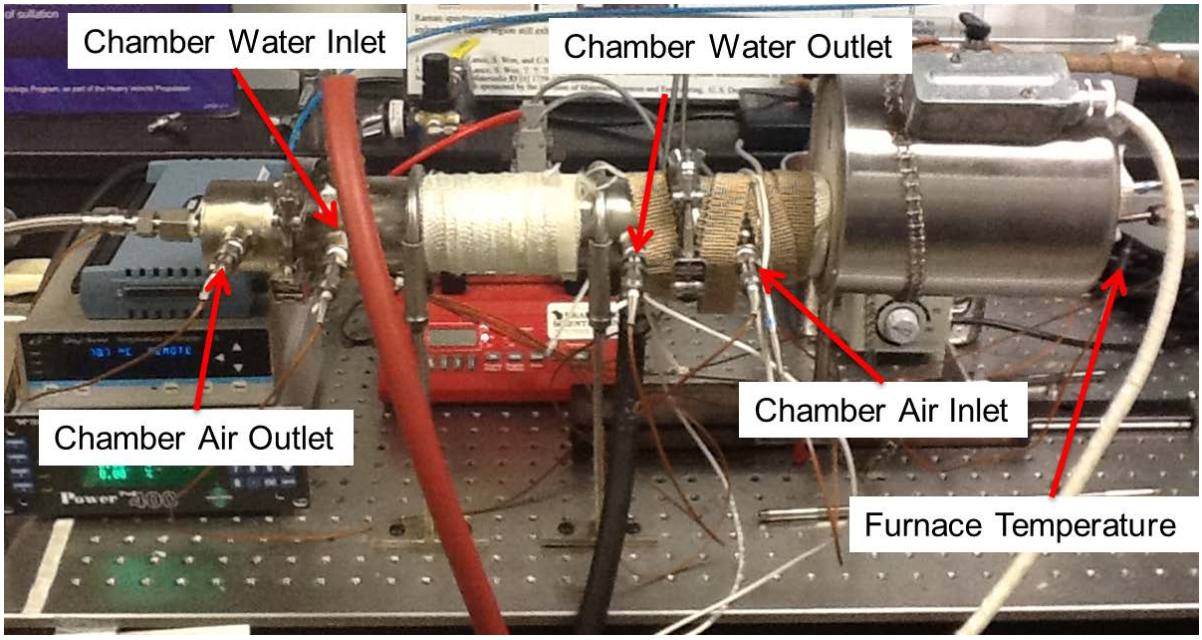

Figure 1. Bench-top tube reactor showing the thermocouple locations.

The effectiveness of the heat exchanger in cooling an empty tube was tested under five different conditions listed in Table 1. As shown in Figure 2, the inlet gas temperature exceeded 400°C at one point which is high enough to simulate common inlet temperatures for light-duty diesel applications. The effectiveness of the heat exchanger was above 90% for the empty tube under all conditions, however, a fouled tube was measured to be 89.6% effective which shows that the presence of the deposit makes it harder to cool the gas. Lower flow rates tended to decrease the inlet gas temperature

due to the longer residence time of the gas prior to entering the heat exchanger, resulting in more gas cooling.

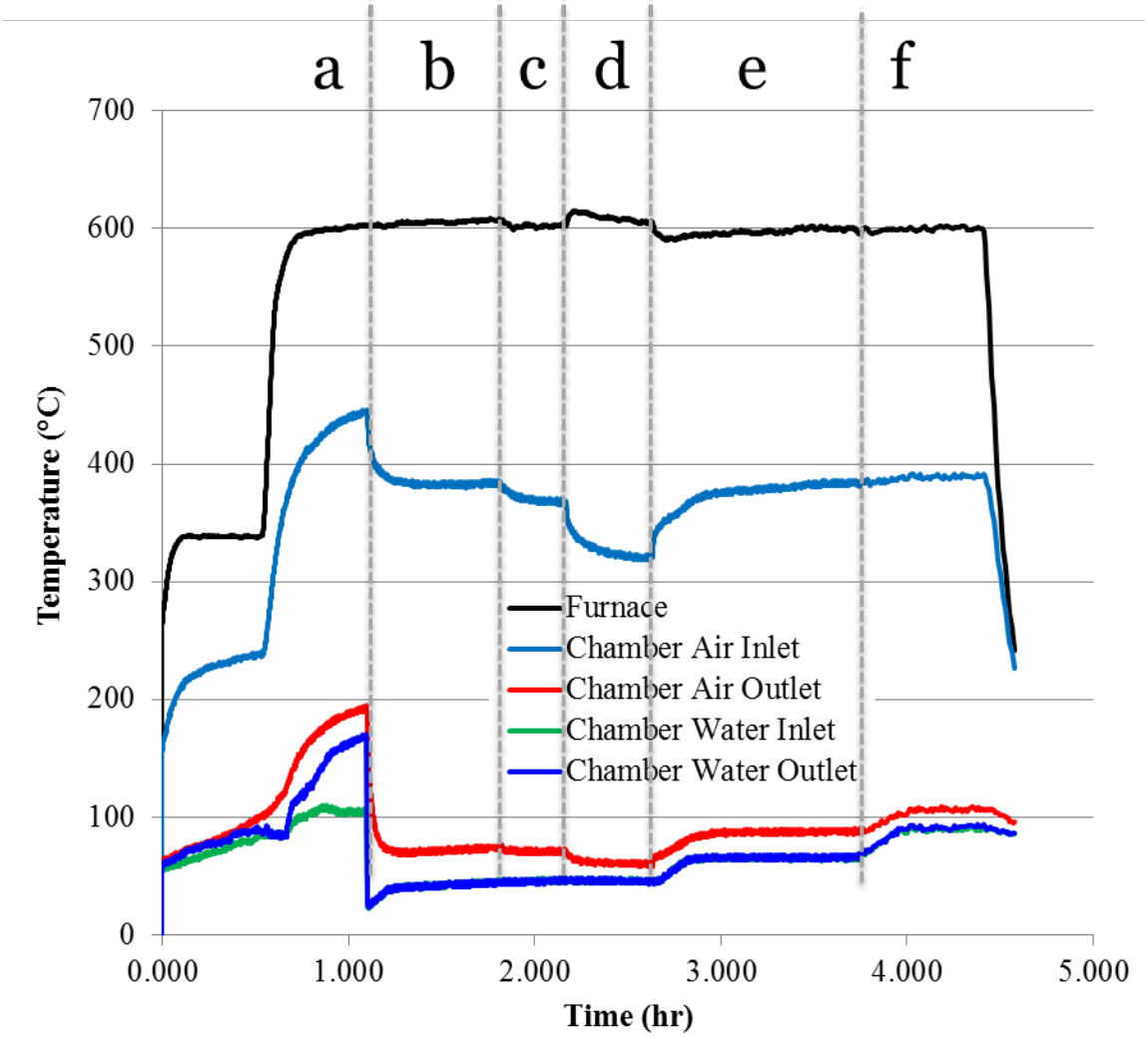

Figure 2. The temperature measured in 5 locations under 5 different conditions (B-F) that simulate different engine operating conditions. The conditions are listed in Table 1.

Table 1: Conditions used to generate the data in Fig. 1. An additional run was performed on a fouled tube in order to show the loss of effectiveness due to the presence of a deposit.

Loaction on Figure 2	Condition	Air Flow (SLPM)	Coolant Temperature (°C)	Furnace Temperature (°C)	Inlet Gas Temperature (°C)	Outlet Gas Temperature (°C)	Effectiveness (%)
B	Empty	20.0	45.0	606.3	383.2	74.8	91.2
C	Empty	15.0	44.9	600.7	369.4	69.0	92.6
D	Empty	10.0	45.5	606.8	320.5	61.0	94.3
E	Empty	15.0	65.1	599.5	383.3	87.2	93.0
F	Empty	15.0	91.1	600.7	389.6	106.1	95.0
Not Shown	Fouled	15.0	43.8	595.9	360.6	76.9	89.6

In addition to the laboratory tests, seven coolers have arrived for the second round of forensic deposit analysis from the industry consortium of EGR technicians. These coolers have all been opened up and the soot is currently being analyzed using TGA and optical and electron microscopy.

Two new pieces of equipment were installed in the previous quarter; a Keyence digital microscope and optical profiler and a TA Instruments Q5000IR thermogravimetric analyzer (TGA).

Status of FY2012 Milestones

1. Using facilities at the High Temperature Materials Laboratory, complete forensic analysis of industry-provided EGR cooler deposits in order to enable better understanding of fouling deposits properties for specific applications (i.e., an idling school bus) so as to meet Tier 4 emission standards of 0.40 g NO_x/kWh with no efficiency penalty. **(09/12)** *On Schedule*
2. Age laboratory-generated deposits (heavy-duty and light-duty) in controlled environments to investigate changes in deposit properties with the aim of increasing the baseline thermal conductivity of 0.04 W/mK to 0.2 W/mK by condensing water and/or HC on the deposit. **(09/12)** *On Schedule.*

Communications/Visits/Travel

None.

Problems Encountered

None.

Publications/Presentations/Awards

J.M.E. Storey, C.S, Sluder, M.J. Lance, D. Styles, and S. Simko, “Exhaust Gas Recirculation Cooler Fouling in Diesel Applications: Fundamental Studies, Deposit Properties and Microstructure,” accepted for publication to Heat Transfer Engineering (2012).

References

None.

Agreement 10635: Catalysis by First Principles

C. Narula, M. Moses DeBusk, Xiaofan Yang
Oak Ridge National Laboratory

Objective/Scope

This research focuses on an integrated approach between computational modeling and experimental development, design and testing of new catalyst materials, that we believe will rapidly identify the key physiochemical parameters necessary for improving the catalytic efficiency of these materials. The results will have direct impact on the optimal design, performance, and durability of supported catalysts employed in emission treatment; e.g., lean NO_x catalyst, three-way catalysts, oxidation catalysts, and lean NO_x traps etc.

The typical solid catalyst consists of nano-particles on porous supports. The development of new catalytic materials is still dominated by trial and error methods, even though the experimental and theoretical bases for their characterization have improved dramatically in recent years. Although it has been successful, the empirical development of catalytic materials is time consuming and expensive and brings no guarantees of success. Part of the difficulty is that most catalytic materials are highly non-uniform and complex, and most characterization methods provide only average structural data. Now, with improved capabilities for synthesis of nearly uniform catalysts, which offer the prospects of high selectivity as well as susceptibility to incisive characterization combined with state-of-the science characterization methods, including those that allow imaging of individual catalytic sites, we have compelling opportunity to markedly accelerate the advancement of the science and technology of catalysis.

Computational approaches, on the other hand, have been limited to examining processes and phenomena using models that had been much simplified in comparison to real materials. This limitation was mainly a consequence of limitations in computer hardware and in the development of sophisticated algorithms that are computationally efficient. In particular, experimental catalysis has not benefited from the recent advances in high performance computing that enables more realistic simulations (empirical and first-principles) of large ensemble atoms including the local environment of a catalyst site in heterogeneous catalysis. These types of simulations, when combined with incisive microscopic and spectroscopic characterization of catalysts, can lead to a much deeper understanding of the reaction chemistry that is difficult to decipher from experimental work alone.

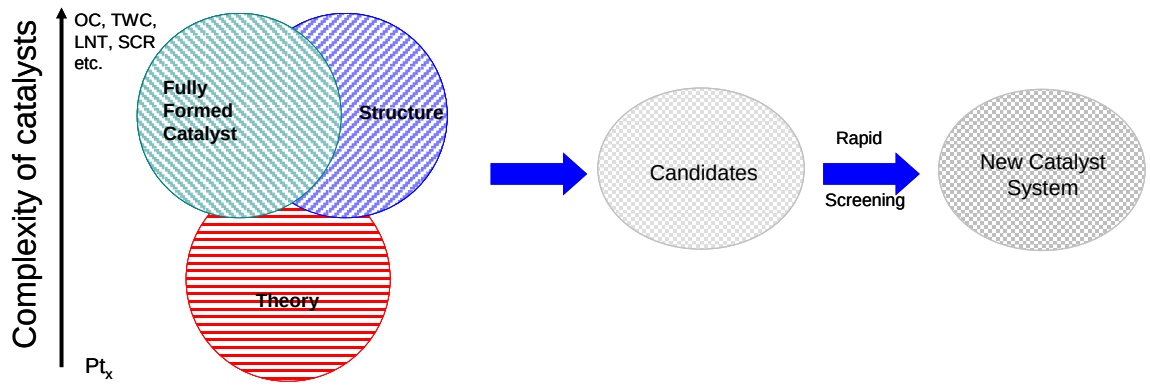

Thus, a protocol to systematically find the optimum catalyst can be developed that combines the power of theory and experiment for atomistic design of catalytically active sites and can translate the fundamental insights gained directly to a complete catalyst system that can be technically deployed.

Although it is beyond doubt computationally challenging, the study of surface, nanometer-sized, metal clusters may be accomplished by merging state-of-the-art, density-functional-based, electronic-structure techniques and molecular-dynamic techniques. These techniques provide accurate energetics, force, and electronic information. Theoretical work must be based on electronic-structure methods, as opposed to more empirical-based techniques, so as to provide realistic energetics and direct electronic information.

A computationally complex system, in principle, will be a model of a simple catalyst that can be synthesized and evaluated in the laboratory. It is important to point out that such a system for experimentalist will be an idealized simple model catalyst system that will probably model a “real-world” catalyst. Thus it is conceivable that “computationally complex but experimentally simple” systems can be examined by both theoretical models and experimental work to forecast improvements in catalyst systems.

We have focused on the oxidation catalyst and SCR catalyst to develop and demonstrate catalyst by design protocol as a prelude to developing catalyst by design protocols for complex emission treatment catalysts; e.g., TWCs, NO_x traps, and HC-SCR catalysts. Our goals are as follows:

- Our theoretical goal is to carry out the calculation and simulation of realistic supported Pt nanoparticle systems (i.e., those equivalent to experiment), in particular by addressing the issues of complex cluster geometries on local bonding effects that determine reactivity. As such, we expect in combination with experiment to identify relevant clusters, and to determine the electronic properties of these clusters. In addition, we plan to study zeolite structures with a view to develop an insight on the mechanistic aspects of catalytic process to enable us to develop better catalysts.
- Our experimental goal is to synthesize metal carbonyl clusters, decarbonylated metal clusters, sub-nanometer metal particles, and metallic particles (~5 nm) on

alumina (commercial high surface area, sol-gel processed, and mesoporous molecular sieve), characterize them employing modern techniques including Aberration Corrected Electron Microscope (ACEM), and evaluate their CO, NO_x, and HC oxidation activity. Furthermore, guided by theoretical studies we plant to synthesize new zeolites and characterize them.

- This approach will allow us to identify the catalyst sites that are responsible for CO, NO_x, and HC abatement. We will then address design of new durable catalysts systems that can withstand the prolonged operations.

Technical Highlights

Until recently, our theoretical studies have focused on supported noble metals. We have shown that single platinum atoms supported on θ-alumina slab are in the zero oxidation state. This result is very different from that reported in literature on single platinum atoms supported on α-alumina or simplified models of γ-alumina where a platinum atom generally has an unpaired electron. This also means that the mechanism of CO, NO_x, or HC oxidation on Pt(0) will be different from that on Pt(I) or Pt(II). We plan to carry out first principle studies of CO oxidation on Pt atoms supported on θ-alumina slab.

Since our experimental work has already shown that the distribution of platinum on γ-alumina and θ-alumina is almost identical, and the surface properties and CO oxidation of both catalysts are identical, we propose that Pt supported on θ-alumina is a better model for Pt supported on γ-alumina than Pt supported on α-alumina or simplified models of γ-alumina.

We have also shown that incorporation of palladium in platinum particles at sub-nanometer scale is quite ineffective in improving the durability, however, large Pt-Pd nanoparticles tend to be more hydrothermally durable than pure Pt particles. While efforts are in progress to prepare sub-nanometer Pt-Pd particles to validate the results of theoretical studies, we have initiated theoretical studies of SCR-zeolite-catalysts.

In this report, we describe our theoretical and experimental studies on single atoms of CO oxidation on Pt/ θ-alumina. Preliminary work on CO oxidation was reported in FY11 annual report. Now, we have completed the optimization of various intermediates and also synthesized and characterized catalyst with single Pt atoms supported on θ-alumina.

Theoretical Studies

CO Oxidation on Pt/θ-alumina (010) surface

As mentioned in the previous reports, platinum supported on θ-alumina (010) surface is in the zero oxidation state with a d^{10} structure and bonded to two oxygen atoms. The implication of this important result is that the mechanism of CO, NO, or HC oxidation on sub-nanometer particles such as single atoms can be expected to be different from the large particles normally examined by DFT. Here, we present our results for the pathways of CO oxidation on a single Pt atom supported on θ-alumina.

While Pt on a dry θ-alumina surface can be stable for indefinite period under oxygen free conditions, it will oxidize readily if any oxygen is present. Since experimentalist will start with oxidized sample, we explored platinum oxidation pathways before CO oxidation. Oxygen can bond to Pt in two possible ways – terminal or side-on. The energetics shows that the side-on configuration is lower in energy than the terminal one. Density of state analysis shows that 5 d_{xy} of Pt and $2p_x$ of O_2 have no electrons. This suggests a d^8 oxidation state for Pt. This structure also draws support from organometallic chemistry where a platinum(0) in a sixteen electron complex, $(Ph_3P)_2Pt(O_2)$, has been shown to exhibit side on configuration by single crystal X-ray crystal structure determination [1]. The absorption energy of O_2 on Pt on a dry θ-alumina surface is -43.20 Kcal/mole.

The oxygen on platinum in $(Ph_3P)_2Pt(O_2)$, has been suggested to dissociate to form Pt=O bond before reaction with CO or a SN2 type CO reaction can occur on Pt with CO bond formation resulting in the oxygen becoming terminally bonded. The formation of carbonate from this structure is quite likely and has been confirmed in the reaction of $(Ph_3P)_2Pt(O_2)$ with CO. The loss of CO_2 from this structure will generate intermediate species containing Pt=O bond which can react with another molecule of CO. This intermediate will form platinum(0) after CO_2 elimination. In analogy with this scheme in homogenous catalysis, we examined possible intermediates for CO oxidation over Pt on a dry θ-alumina surface.

On a reduced Pt surface, the CO absorption can occur with bond formation between Pt and the carbon of CO. There is no magnetic moment associated with this structure and the density of state analysis shows it to be in d^{10} oxidation state. All d orbitals of Pt are filled and bonding is through σ_C of C=O. The absorption energy of CO on Pt on a dry θ-alumina surface is -43.06 Kcal/mole. Since there is no significant difference between CO and O_2 absorption energy, CO and oxygen can compete for the platinum(0) site.

Regardless of whether the first species formed is Pt with O_2 absorbed on it or CO, the next intermediate forms with the bonding of both CO and O_2 on the same Pt atom. This intermediate formation involves breaking of one Pt-O bond with the surface. The intermediate is still a d^{10} system with magnetization at oxygen atoms of O_2 species. The absorption energy for oxygen is -45.79Kcal/mole. This intermediate undergoes rearrangement to form a carbonate species. The carbonate species is a d^8 species with no magnetization. DOS analysis shows no electrons in Pt $5d_{xy}$ and $C2p_z$. This species is analogous to an organometallic platinum(0) sixteen electron complex, $(Ph_3P)_2Pt(CO_3)$, which has been shown to exhibit CO_3 bonding via two oxygen atoms by single crystal X-ray crystal structure determination [2].

The elimination of CO_2 from the carbonate species forms a monoxide high spin d^8 species. DOS shows Pt d_{xy}, Pt d_{yz}, O1 p_z, and O1p_x partially occupied. The DOS of p-orbitals of the alumina surface oxygen atoms bonded with platinum are shifted to lower energy and have features similar to parent compound.

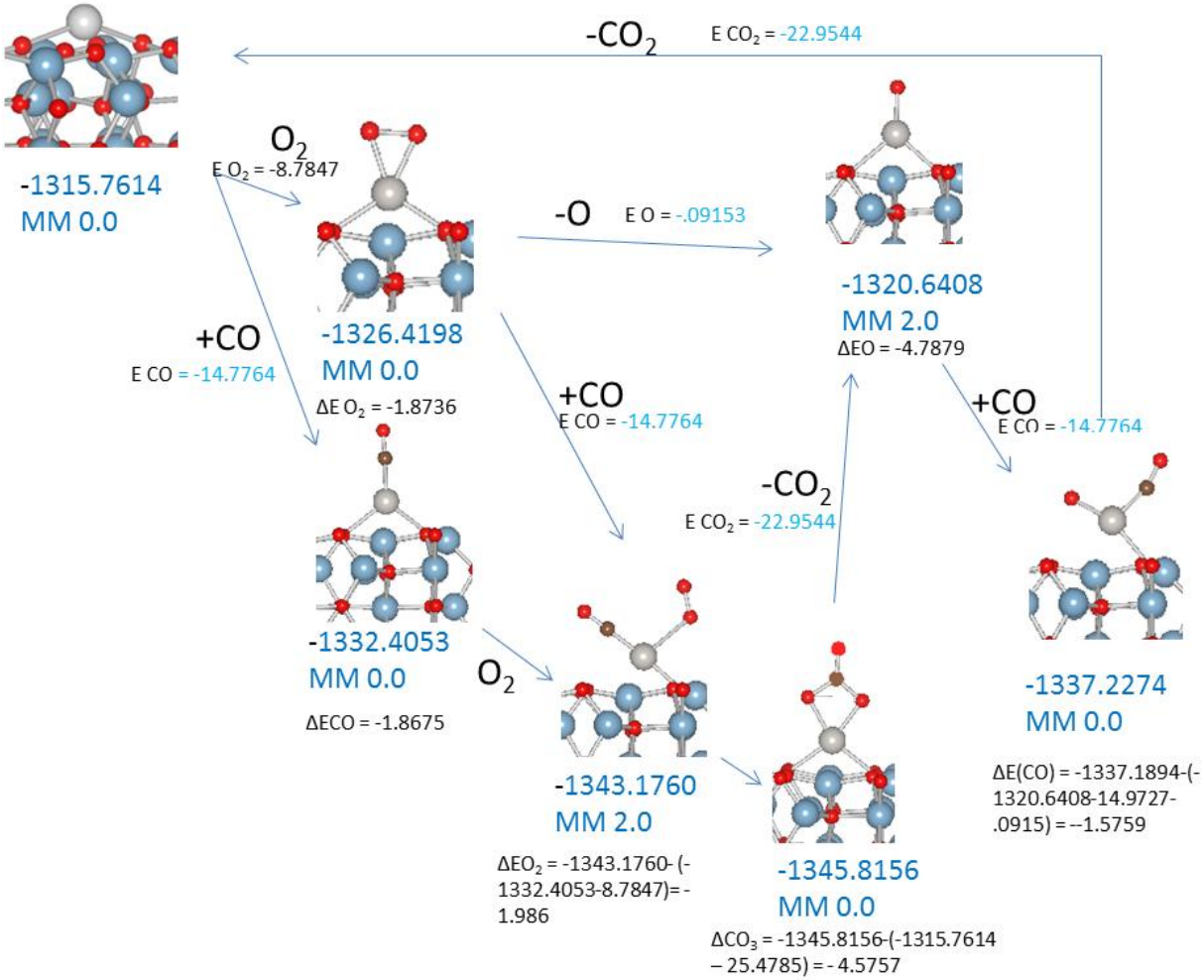

The monoxide complex reacts with CO to form a new intermediate which eliminates CO_2 to furnish the catalyst that can start a new catalytic cycle for CO oxidation.

Experimental Studies:
In order to validate the results of theoretical modeling studies, we have attempted to synthesize Pt/theta-alumina with Pt distributed on alumina surface as single atoms. The samples were prepared by impregnation method with Pt loading of 0.18% and 1%. The EXAFS studies suggest that 0.18% sample is most probably comprised of single Pt atoms on the alumina surface.

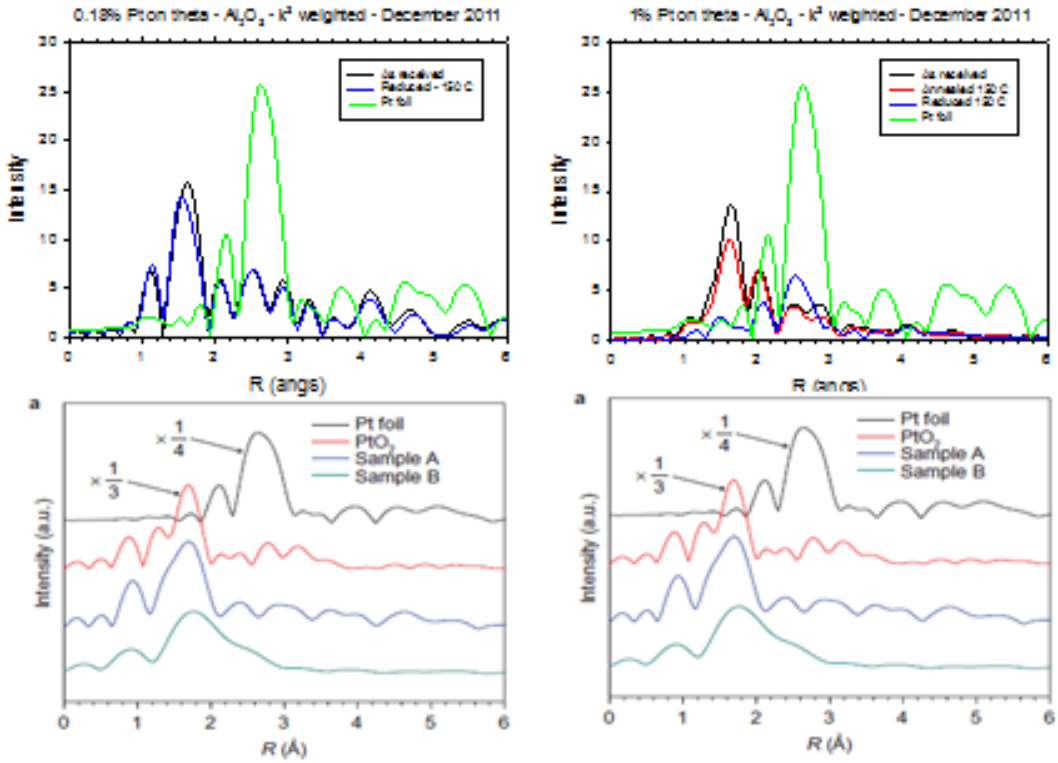

EXAF of 0.18% (top-left) and 1% Pt (top-right) on theta-alumina; the figure on bottom left and right are from literature for comparison where sample A is 0.18% and sample B is 2% Pt on iron oxide from ref 3.

The EXAFS of our samples were recorded on fresh samples and after reducing them at 150C under a flow of hydrogen. The 0.18% sample shows peaks near 2Å for Pt-O bond but there are no peaks at 2.8Å normally assigned to Pt-Pt bonds. The 1% sample does not exhibit Pt-Pt bond either when fresh suggesting all Pt is oxidized. However reduction step leads to a new peak in EXAFS near 2.8 A normally assigned to Pt-Pt bond. Further studies are in progress by IR and electron microscopy to ascertain these results. We will carry out CO oxidation studies if the IR and TEM data on 0.18% sample confirm it to contain only single atoms.

<u>Status of FY2012 Milestones</u>:

1. We will complete theoretical modeling of large supported Pt clusters by Sept 2012 resulting in a thorough understanding of subnanometer Pt and Pt clusters supported on alumina.

We have completed modeling of 2 atom clusters and larger cluster analysis is in progress.

2. This information will be used to initiate mechanistic studies of CO, NO_x and HC oxidation on Pt/alumina and heterobimetallic zeolites.

   The CO oxidation on Pt single atoms results are described in this report.

Communication/Visits/Travel

We have prepared a manuscript titled "Ab Initio Density Functional Calculations of Adsorption of Transition Metal Atoms on θ-Al_2O_3(010) Surface" has been recommended for publication in Journal of Physical Chemistry, C after revision. We have completed the revision and are resubmitting the manuscript.

Problems Encountered

none.

Publications

1. C.K. Narula, M.G. Stocks, "Ab Initio Density Functional Calculations of Adsorption of Transition Metal Atoms on θ-Al_2O_3(010) Surface" J. Phys. Chem,. C (manuscript recommended for publication after revision).
2. C.K. Narula, "Catalyst by Design – Bridging the Gap between Theory and Experiments at Nanoscale Level" Encyclopedia of Nanoscience and Nanotechnology, Vol. II, Taylor & Francis, New York, 2008, pp 771-782 (invited).
3. C.K. Narula, L.F. Allard, D.A. Blom, M. Moses-DeBusk, "Bridging the Gap between Theory and Experiments – Nano-structural Changes in Supported Catalysts under Operating Conditions" SAE-2008-01-0416, SAE Int. J. Mater. Manu., 1(2008) 182-188.
4. C.K. Narula, L.F. Allard, D.A. Blom, M.J. Moses, W. Shelton, W. Schneider, Y. Xu, "Catalysis by Design - Theoretical and Experimental Studies of Model Catalysts", SAE-2007-01-1018 (invited).
5. C.K. Narula, M.J. Moses, L.F. Allard, "Analysis of Microstructural Changes in Lean NO_x Trap Material Isolates Parameters Responsible for Activity Deterioration" SAE 2006-01-3420.
6. Y. Xu, W.A. Shelton, and W.F. Schneider, "The thermodynamic equilibrium compositions, structures, and reaction energies of Pt*x*O*y* (*x* = 1-3) clusters predicted from first principles," *Journal of Physical Chemistry B,* 110 (2006) 16591.
7. Y. Xu, W. A. Shelton, and W. F. Schneider, "Effect of particle size on the oxidizability of platinum clusters," *Journal of Physical Chemistry A*, 110 (2006) 5839.
8. C.K. Narula, S. Daw, J. Hoard, T. Hammer, "Materials Issues Related to Catalysts for Treatment of Diesel Exhaust," *Int. J. Amer. Ceram. Tech*., 2 (2005) 452 (invited).

Presentations (last 12 months)

1. Narula, C.K. Stocks, G.M., Density Functional Studies of Adsorption of Transition Metal Atoms on θ-Al_2O_3(010) Surface" American Chemical Society Meeting, Denver, CO, August 28, 2011.

2. Narula, C.K.; Stocks, M. G.; First-principles studies of the structure and bonding of metal atoms supported on θ-alumina, American Chemical Society Meeting, San Francisco, March 2010.
3. Narula, C.K.; Chen, X.; Stocks, G.M., DeBusk, M.M.; Allard, L.F.; "First-Principles and Experimental Studies of the Sub-Nanometer Platinum Atoms Supported on θ-Alumina" 230th American Chemical Society Meeting, Boston, MA, August 22-26, 2010

References

1. Cheng, P.T.; Cook, C.D., Nyburg, S.C., Wan, K.; Can. J. Chem., 49 (1971) 3772.
2. Scholz, S.; Lerner, H.W.; Bolte, M. Acta Cryst E62 (2006) m312-m313. Gregg, M.R.; Powell, J.; Sawyer, J.F.; Acta. Crystal. C44 (1988) 43-46
3. Qiao, B; Wagn, A.; Yang, X.; Allard, L.F.; Jiang, Z.; Cui, Y.; Liu, J.; Li, J.; Zhang, T.; Nature Chem., 3 (2011) 634

Agreement 19214: Effects of Biodiesel Fuel on Diesel Particulate Filter Materials

M. J. Lance, B. J. Bunting, A. A. Wereszczak, E. E. Fox, and T. J. Toops
Oak Ridge National Laboratory

Objective/Scope

To characterize changes in the microstructure and material properties of diesel particulate filters (DPFs) in exhaust gas produced by biodiesel blends.

Technical Highlights

Additional mechanical testing of a 25-mm diameter DPF ceramic was completed during the present reporting period. Summaries of the results for all the 25-mm DPFs tested to date are listed in Tables 1-3. Three mechanical test methods and their methods were described in the FY11 Annual Report and will be published in a proceedings paper as part of the 2012 International Conference on Advanced Ceramics and Composites (ICACC).

Table I. Summary of biaxial flexure testing results. Nominal disk thickness is 1.5 mm. Ring diameters are 6.75 and 16 mm. Values in parenthesis are one standard deviation.

Material	Average Flexure Failure Force (N)
Cordierite C611-HG 59% Porosity Center	0.6 (± 0.4)
Cordierite C611-HG 59% Porosity End	1.6 (± 1.1)
Cordierite C611 59 % Porosity Center	2.3 (± 0.4)
Cordierite C611 59 % Porosity End	3.0 (± 0.8)
SiC	7.2

MSC-111 53% Porosity Center	(± 1.4)
SiC MSC-111 53% Porosity End	13.7 (± 4.1)
SiC MSC-14 58% Porosity Center	6.1 (± 1.4)
SiC MSC-14 58% Porosity End	11.1 (± 1.6)

Table II. Summary of sectored flexure testing results. Nominal thickness is 4 mm. Four-point-bend spans are 30 and 60 mm. Values in parenthesis are one standard deviation.

Material	**Average Flexure Failure Force (N)**
Cordierite C611-HG 59% Porosity 0° orientation	8.8 (± 0.5)
Cordierite C611-HG 59% Porosity 45° orientation	8.1 (± 0.7)
Cordierite C611 59 % Porosity 0° orientation	7.2 (± 0.5)
Cordierite C611 59 % Porosity 45° orientation	7.4 (± 1.5)

SiC MSC-111 53% Porosity 0° orientation	34.6 (± 3.6)
SiC MSC-111 53% Porosity 45° orientation	34.0 (± 3.8)
SiC MSC-14 58% Porosity 0° orientation	Not measured yet
SiC MSC-14 58% Porosity 45° orientation	28.2 (± 3.5)

Table III. Summary of o-ring testing results. Nominal thickness is 5 mm. Values in parenthesis are one standard deviation.

Material	**Average Failure Initiation Force (N)**
Cordierite C611-HG 59% Porosity 0° orientation	4.0 (± 1.3)
Cordierite C611-HG 59% Porosity 45° orientation	3.2 (± 0.9)
Cordierite C611 59 % Porosity 0° orientation	3.9 (± 0.8)
Cordierite C611 59 % Porosity 45° orientation	3.2 (± 0.9)
SiC MSC-111 53% Porosity 0° orientation	15.8 (± 6.9)
SiC	11.4

MSC-111 53% Porosity 45° orientation	(± 0.6)
SiC MSC-14 58% Porosity 0° orientation	13.1 (± 6.4)
SiC MSC-14 58% Porosity 45° orientation	8.3 (± 1.4)

The generator set for thermal cycling has been installed and started up. Shakedown testing indicated the need for a complete change of exhaust system due to the use of a glass-pack muffler which shed fibers and face-plugged the DPF and due to excess cooling of exhaust, which was done by the manufacturer for safety of outdoor installations. These two problems have been corrected by a complete rebuild of the exhaust system (shown in Fig 1). Thermal cycling of the diesel particulate filter is done by a combination of generator set load and exhaust fuel injection and can reach temperatures of about 700°C in a 15 minute cycle.

Figure 1. Pictures of the generator set installation and a view of the outlet side of the DPF during active regeneration.

Work for next quarter will include installing a larger fuel tank for 24 hour operation, possible further modifications to the exhaust system, further development of the test cycle, control, and data acquisition, and calibration of the DPF for backpressure vs. soot loading.

Status of FY 2012 Milestones

1. Establish baseline mechanical testing of DPFs by measuring the elastic modulus and fracture strength of both the skin and interior of the DPF of both SiC (with 52 and 58% porosity) and cordierite (13 and 18 µm pore size) materials with at least 12 samples so as to determine fracture (Weibull) statistics. **(12/11)** *On schedule*
2. Age filter samples with Na and K doping in order to simulate long-term biodiesel exposure as dictated by the ASTM D6951 to 5 ppm and measure degradation using testing procedure developed in Milestone 1. **(9/12)** *On Schedule*

Communications/Visits/Travel:

CLEERS teleconference (November 17th) presentation entitled "Failure Stress and Apparent Elastic Modulus of Diesel Particulate Filter Ceramics"

Problems Encountered

None.

Publications/Presentations/Awards

E. E. Fox, A. A. Wereszczak, M. J. Lance, and M. K. Ferber, "Failure Stress and Stiffness Analysis of Ceramic From a 25-mm Diameter Diesel Particulate Filter," proceedings paper submitted to, and presented at, the 36th International Conference and Exposition on Advanced Ceramics and Composites, Daytona Beach, FL, January 23-26, 2012.

References

None.

Agreement 20091: Electrically Assisted DPF Material

M. J. Lance, J. E. Parks, A. A. Wereszczak, W. P. Partridge, E. E. Fox, and M. K. Ferber
Oak Ridge National Laboratory

Objective/Scope

In this CRADA project with General Motors (GM), two research objectives are being pursued:

1. Measure of substrate temperatures during DPF regeneration with optically based techniques that are not susceptible to conductive interferences that are problematic for common thermocouple technologies.
2. Analysis of diesel particulate filter (DPF) substrate materials to understand crack and failure mechanisms and resolve current differences in simulation and experimental results.

Technical Highlights

To attempt to confirm this project's earlier reporting of the DPF cordierite having an elastic modulus of 1-2 GPa (measured with biaxial flexure, sectored flexure, and o-ring compression testing), thin test coupons of isolated cordierite were carefully harvested out of DPFs and then loaded in three point bending. These specimens were very fragile so care was taken to cause sufficient bending prior to their fracture. An example of this test is shown in Fig. 1. The three-point-loading enabled the use of classical beam bending analysis with measurement of the applied compressive force and corresponding load-point-deflection. An elastic modulus of approximately 1 GPa was representative of that force-deflection bending response, and that is consistent with the authors' earlier reported values. This provides additional confirmation that this elastic modulus of about 1 GPa is an accurate portrayal of DPF cordierite stiffness, and that resonance-based values of elastic modulus (about an order of magnitude larger) are misleadingly high.

Status of FY 2012 Milestones

(1) Measurement of the wall temperature of the DPF at 8 different locations with a spatial resolution of 1 mm and temperature accuracy of +/- 10°C during regeneration at typical operating conditions (600-800 C) using a fiber optic technique. (09/2012) *On Schedule*

(2) Creation of DPF samples with a temperature exposure history equivalent to 15000 miles of operation on a light-duty vehicle for analysis by the MST team. (09/ 2012) *On Schedule*

(3) Measure retained strength of laboratory-exposed DPF specimens (provided by FEERC Team from Milestone 2) and extrapolate to the degradation expected from a lifetime of electrically-assisted regenerations (~700 cycles) in order to determine if the improvement in engine efficiency from this technology is worth the potential decrease in substrate lifetime. (09/2012) *On Schedule*

Communications/Visits/Travel
2011 Directions in Engine-Efficiency and Emissions Research (DEER) Conference, Detroit, MI, October 3-6, 2011.

Problems Encountered
None.

Publications/Presentations/Awards
Andrew A. Wereszczak, Michael J. Lance, and Ethan E. Fox, "Failure Stress and Apparent Elastic Modulus of Diesel Particulate Filter Ceramics," poster presentation given at 2011 Directions in Engine-Efficiency and Emissions Research (DEER) Conference, Detroit, MI, October 3-6, 2011.

A. A. Wereszczak, M. J. Lance, E. E. Fox, and M. K. Ferber, "Failure Stress and Apparent Elastic Modulus of Diesel Particulate Filter Ceramics," teleconference presentation given to US DOE Crosscut Lean Exhaust Emissions Reduction Simulation (CLEERS) monthly meeting, 17 November 2011.

A. A. Wereszczak will give a presentation to the C28 Advanced Ceramics Committee on the DPF mechanical test coupons developed in this project, January 22, 2012.

A. A. Wereszczak, E. E. Fox, M. J. Lance, and M. K. Ferber, "Failure Stress and Apparent Elastic Modulus of Diesel Particulate Filter Ceramics," manuscript submitted and to be presented at the SAE 2012 World Congress, Detroit, MI, April 24-26, 2012.

References
None.

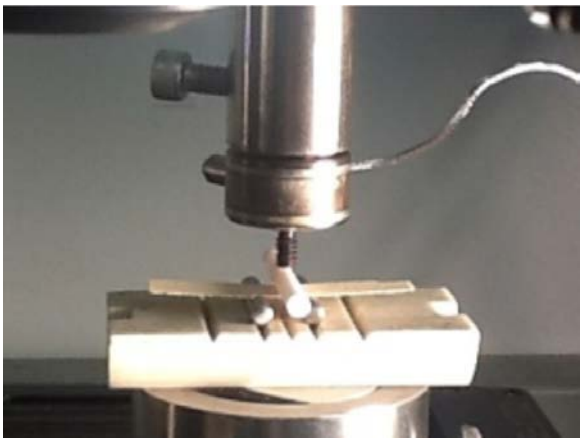

Figure 1. Thin slice of DPF cordierite subjected to three point bend testing. The shown amount of bending (caused by only a 0.15 N compressive force) is consistent with an elastic modulus of approximately 1 GPa.

Agreement 9105: Characterization of Catalyst Microstructures

L.F. Allard, C.K. Narula, W.C. Bigelow, M.B. Katz, X. Pan, G. W. Graham, D.P. Nackashi and J. Damiano
Oak Ridge National Laboratory

Objective/Scope

The objective of the research is to understand fundamental processes in catalytic systems with applications to transportation technologies, such as those used for the treatment of NO_X emissions, and for the production of biomass-derived liquid fuels. The research heavily utilizes new capabilities and techniques for ultra-high resolution transmission electron microscopy with the HTML's aberration-corrected electron microscope (ACEM). The research is ultimately focused on understanding the effects of reaction conditions on the changes in morphology of heavy metal species on "real" catalyst support materials (e.g. oxides and carbon materials), and the understanding of the structures of model mono-, bi- and multi-metallic catalyst systems of known particle composition. A major thrust of these studies has been to develop methods of *in situ* microscopy at elevated temperatures and under controlled gas compositions. We have worked for some time with Protochips Inc. (Raleigh, NC), which provides a novel heating technology utilizing MEMS-based heating devices that we have shown to be stable enough to provide sub-Ångström imaging capabilities at high temperature in the ACEM. The devices have permitted the recent development of a closed-cell gas reaction holder that allows heating under controlled gas compositions up to a full atmosphere, with the ability to image atomic structure under these conditions. Methods using the new reactor, or "E-cell" (environmental cell), are currently being employed in a new study of "intelligent catalysts" for automotive emission control applications, based on the reported self-regenerative phenomenon of heavy metal species such as Pd and Rh in Ca- and La-based perovskite crystal structures. This work is being conducted in collaboration with Prof. Xiaoqing Pan of the University of Michigan, and his student Michael Katz and colleague George Graham, with further collaboration with Ford Research Laboratory colleague Dr. Andrew Drews.

Technical Progress

The Daihatsu 'intelligent catalyst' [1] has been promoted as one solution to the problem of precious metal particle coarsening in automotive catalysts. In this material, the precious metal cyclically dissolves and extrudes from a specially selected perovskite support upon exposure to oxidizing and reducing conditions, respectively. The mechanistic nature of these systems has been the object of numerous studies over the past several years, typically via EXAFS and XANES spectroscopic analysis methods to ascertain the average structure of the catalyst. We are using our *in situ* microscopy techniques for direct imaging of catalytic processes in these systems under realistic reaction conditions.

In recent work at the University of Michigan, studying two proposed 'intelligent catalyst' systems, Pt-doped $CaTiO_3$ (CTO) (and other precious-metal-doped perovskite) model thin-film cross sections were characterized using aberration-corrected STEM

techniques. These studies found that the situation is much more complex [2,3]. For instance, when Pt-CTO is reduced in simulated engine conditions, Pt does not primarily exit the perovskite host, but rather forms internal particles and clusters of varied character. Conversely, when re-oxidized, the smallest Pt clusters apparently dissolved, but the majority of Pt species remained as small internal metallic particles. Any Pt appeared to extrude onto a free surface during reduction simply coarsened upon re-oxidation. The conclusion was that it is likely that the incompleteness of the oxidizing half of the reaction is due either to inappropriate temperatures or insufficient times of reaction.

Further work at ORNL involved high-temperature gas reaction studies in the STEM, using E-cell reaction techniques. Pt-CTO powder was loaded onto a heater device in the gas-cell holder and first examined in its as-prepared state, which comprised generally 50-200 nm single-crystal perovskite primary particles with a sparse dispersion of nascent Pt particles that formed during synthesis (Fig. 1a). During reduction at 800°C in 4% H_2/Ar at 100 Torr, a plurality of small Pt clusters were extruded from the perovskite host (Fig. 1b). This reaction was nearly complete after about 1 min of exposure to reaction conditions, with very little change following. The position of the Pt clusters relative to the perovskite particles was ambiguous due to the projective nature of STEM imaging, but most were presumed to remain within the bulk of the perovskite support, based on the prior results of work with model cross sections [2]. Oxidation at 800 °C in 20% O_2/N_2 followed, but was effective only in inducing a small number of Pt clusters to re-dissolve into the perovskite host after an hour and longer (Fig. 1c,d), again in agreement with our previous findings. Work is currently underway both to explore experimental parameter space in order to find more ideal conditions for re-dissolution of Pt into CTO, and to study other proposed precious-metal/perovskite 'intelligent catalyst' systems.

References

[1] Y. Nishihata *et al.*, "Self-regeneration of a Pd-perovskite catalyst for automotive emissions control," *Nature.* **418** (2002) 164.

[2] M.B. Katz *et al.*, *submitted* (2012).

[3] M.B. Katz *et al.*, "Self-Regeneration of Pd–$LaFeO_3$ Catalysts: New Insight from Atomic-Resolution Electron Microscopy," *J. Amer. Chem. Soc.* **133** (2011) 18090

Status of Milestones

On schedule

Communications/Visits/Travel

Larry Allard presented a talk entitled "Recent Developments in *In Situ* Heating and Gas-Reaction Studies of Catalytic Materials via STEM Imaging in an Aberration-Corrected Electron Microscope," at the MS&T Annual Meeting, Columbus, OH, October 2011. He also co-organized the symposium "Advanced Developments in Electron Microscopy."

Publications

None this quarter.

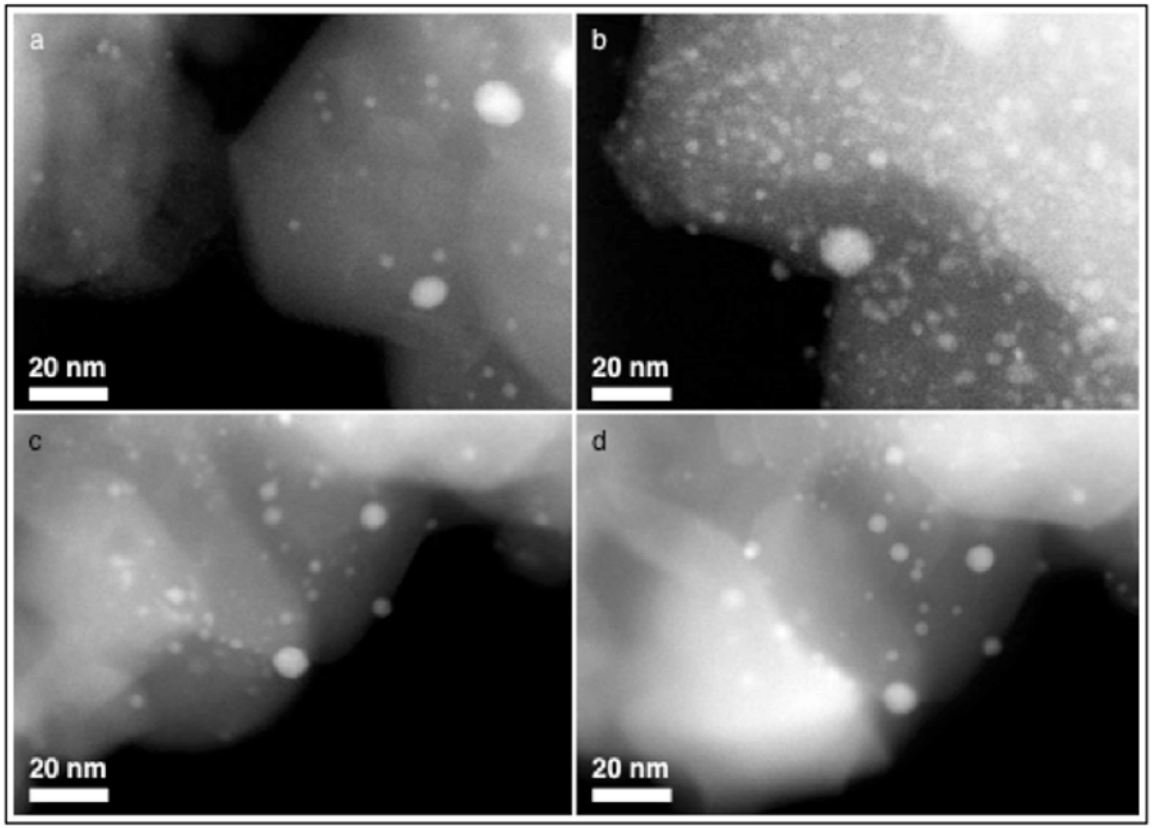

Fig. 1. (a) A typical region of Pt:$CaTiO_3$ powder as-prepared, showing sporadic nascent Pt particles; (b) the same region after 5 min reduction each, first at 600°C then at 800°C, in 4% H_2/Ar; (c) a typical region after reduction; (d) after 100 min of re-oxidation, showing limited re-dissolution of small Pt clusters.

Agreement 14957: High Temperature Thermoelectrics

A. A. Wereszczak,[1] H. Wang,[1] R. McCarty,[2] A. Thompson,[2] and J. Sharp[2]

[1]Oak Ridge National Laboratory
[2]Marlow Industries, Inc.
Dallas, TX 75238

Objective/Scope

Two-thirds of the chemical energy in automotive fuel is rejected to the atmosphere as waste heat. Thermomechanical stresses must be managed and TE material strength must be improved to fully exploit TE devices for waste heat recovery. Toward that, needed thermomechanical and thermophysical properties of candidate thermoelectric (TE) materials are measured in this project and then used with established probabilistic reliability and design models to optimally design automotive and heavy vehicle TE modules. Thermoelectric materials under candidacy for use in TE modules tend to be brittle, weak, and have a high coefficient of thermal expansion (CTE); therefore, they can be quite susceptible to mechanical failure when subjected to operational thermal gradients. A successfully designed TE module will be the result of the combination of temperature-dependent thermoelastic property and strength distribution data and the use of the method of probabilistic design developed for structural ceramics.

Technical Highlights

Mechanical Properties and Supportive Testing

Flexure strength testing of several grades of several Marlow-fabricated bismuth tellurides and zinc sulfides continued in Q1. Numerous dilatometry tests of Marlow-fabricated skutterudites and zinc sulfides were also completed.

In preparation for greater emphasis on the evaluation of device reliability, an ultrasonic tester and a shear tester were acquired. Both are shown in Fig. 1 and will be used in FY12 to evaluate the metallization joints between device substrates and thermoelectric legs.

Transport Property Measurements, Residual Stress, and IEA Activities

Transport property of Marlow materials continued to be characterized for material performance. Thermal conductivity, electrical resistivity and Seebeck coefficient were tested from 20-500°C on research materials and near-production materials for thermoelectric modules.

Residual stresses of Marlow skutterudite modules were evaluated at the High Flux Isotope Reactor (HFIR) during FY12Q1. Stress-free powders of n-type and p-type materials, freestanding thermoelectric legs, production bulk sample and a TE couple were lined up for neutron scattering, shown in Fig. 2. The HFIR data is being analyzed.

Figure 1. New ultrasonic (left) and shear testers (right) will be used to evaluate metallization joint strength.

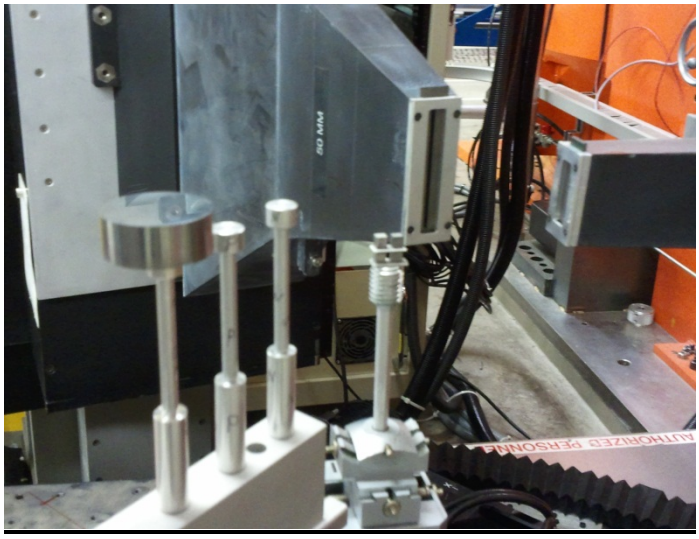

Figure 2. Sample set-up for HFIR neutron residual stress measurements: TE powders were in aluminum tubes, a TE couple was in the beam line with two stress free legs glued on top.

IEA-AMT Annex VIII completed the second round-robin on p-type bismuth telluride on October. The preliminary results were reported to the AMT executive committee in Helsinki Finland in October. An IEA topical report was completed and published in November 2011 by Annex VIII participants on the two international round-robin tests of thermoelectric materials. The annex topical report also included recommended standard testing procedures for transport properties of bulk thermoelectrics.

Status of FY 2012 Milestones

1. Measure mechanical, thermoelastic, and thermoelectric properties of Marlow-fabricated TE materials to enable reliable operation up to 500°C. [Sep12] *On schedule.*
2. Process and engineer sintered bulk polycrystalline Si to reduce its thermal conductivity to less than 10 W/mK. [Sep12] *On schedule.*
3. Complete report of international round-robin test results on Marlow bismuth telluride to IEA-AMT and initiate a new high temperature thermoelectric round-robin measurements on PbTe or skutterudite ranging between 20-500°C. *On schedule.*

Communications/Visits/Travel

- Semi-annual CRADA review with Marlow was held on 16 Nov. 2011 at ORNL.
- IEA-AMT Executive Committee meeting was held in VTT Helsinki, Finland, October 18-19, 2011. H. Wang presented Annex VIII report to the committee.

Problems Encountered: None.

Publications/Presentations/Awards:

1. Hsin Wang, et al., "International Energy Agency Topical Report: Transport Properties of Bulk Thermoelectrics", ORNL Report #32716, November 2011.
2. Hsin Wang, et al., International Energy Agency annual report on Annex VIII, December 2011.

References

None.

Agreement 16308: MBD Thermoelectrics Theory and Structure

David J. Singh
Oak Ridge National Laboratory

Objective/Scope

We will use modern science based materials design strategies to find ways to optimize existing thermoelectric materials and to discover new families of high performance thermoelectrics for waste heat recovery and vehicular cooling applications in vehicles. The emphasis will be on the thermoelectric figure of merit at temperatures relevant to waste heat recovery and vehicular cooling and on other properties important for applications, especially anisotropy, cost and mechanical properties.

Technical Highlights

Vehicular applications of thermoelectric materials for waste heat recovery, as well as room-temperature passenger cooling (necessary for the performance of hybrid electric vehicles) necessitate the study and identification of high performance materials comprised of elements low in cost and abundant, and (for waste heat recovery) with high melting points > 1000 K. Continuing our recent study of such materials, we have performed a detailed technical analysis (performed using WIEN2K [1] and the in-house developed transport code BoltzTrap [2]) of the transition metal silicide $CrSi_2$ (Figure 1), whose melting point is 1711 K. Worldwide annual chromium production exceeds 20 million tons [3], while silicon is abundant, readily available and inexpensive at the purities needed for thermoelectric application.

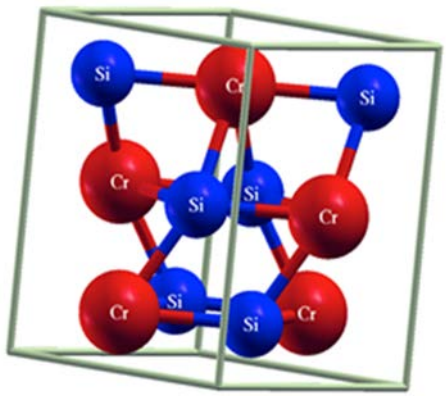

Figure 1. The hexagonal crystal structure of $CrSi_2$, which we found to be a promising material for thermoelectric applications.

$CrSi_2$ has until now not been considered as a useful thermoelectric [4] due to a comparatively high lattice thermal conductivity (about 8 W/m K at 300 K) and small band gap (~ 0.35 eV). Materials with large lattice thermal conductivity are usually not favored [5] as thermoelectrics as a large fraction of their heat transport is carried by phonons and therefore cannot be used to generate electrical current. A small band gap tends to limit the operation regime of the material to low temperature, since at elevated temperatures excitations across the band gap occur and cause greatly increased thermal conductivity and reduced Seebeck coefficient. For these reasons, while the thermoelectric properties of $CrSi_2$ have been studied in a limited way, by and large it has not received the type of detailed, focussed attention necessary to determine its potential thermoelectric performance with optimized doping levels. In this context the insight that our first principles calculations provide, namely at what temperatures and

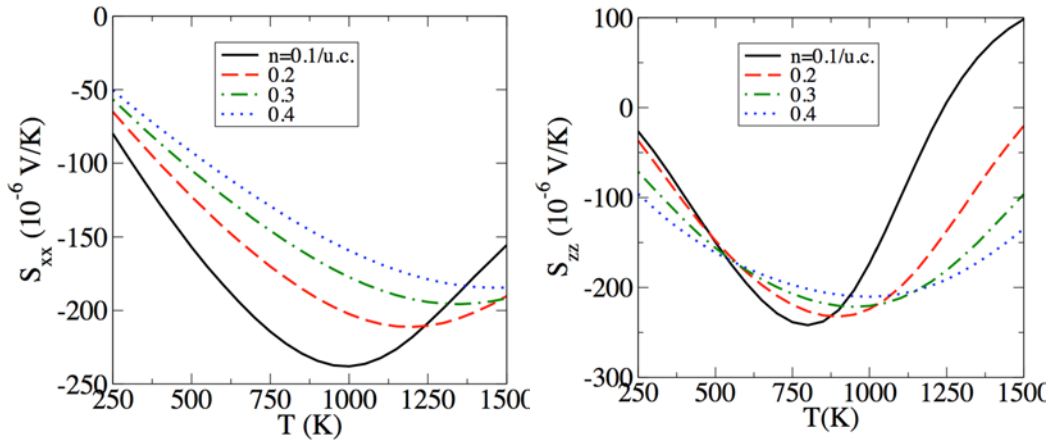

Figure 2. Calculated thermopower, $S(T)$ of $CrSi_2$ at several electron concentrations in the planar (left) and axial (right) directions as a function of temperature. Note that at carrier concentrations of 0.1 to 0.2 high thermopowers of approximately -200 μV/K are found between 800 K and 1000 K.

dopings optimal performance may be found, is expected to be most helpful to experimental groups developing this material for thermoelectric application.

Our approach for $CrSi_2$ is to examine transport at elevated temperatures of 900 K and above, where the lattice thermal conductivity, which decreases with temperature, is less of a concern. This temperature represents the higher end of motor vehicle exhaust temperatures. The effects of the small band gap (ordinarily creating destructive excitations across the band gap at these temperatures) can be mitigated by very heavy dopings, which cause the Fermi level, and hence the electronic structure near the Fermi level, to be more removed from opposite sign conduction.

Figure 2 shows our calculated thermopower, or Seebeck coefficient, for this material for a range of n-type dopings and temperatures. These were obtained using the first principles electronic structure, calculated using the state-of-the-art linearized augmented planewave method with a newly developed modification of the Becke-Johnson potential, and the Boltztrap code, which was co-developed at ORNL. Of note are thermopowers as large in magnitude as 200 μV/K for very heavy dopings of approximately 0.2 electrons per unit cell, or about 1.85 x 10^{21} cm^{-3}, at temperatures between 900 K and 1250 K. Note that the well-known expression for the figure-of-merit ZT [5],

$$ZT = \sigma S^2 T/k,$$

where S is the Seebeck coefficient, T the temperature, σ the electrical conductivity and κ the thermal conductivity (which contains both electronic and phononic components), can be rewritten in the following form, assuming the Wiedemann-Franz relation [6]:

$$ZT=S^2 r/L_0$$

Where r is the ratio of *electronic* thermal conductivity and *total* (i.e. electronic + phononic) thermal conductivity, and L_0 is the Lorenz number, typically equal to about 2.5 x 10^{-8} $(V/K)^2$ (+/-20%). This form implies that even if the lattice thermal conductivity were nil, a Seebeck coefficient of 156 μV/K would be required for a ZT of unity. Since the lattice term is never zero, thermopowers significantly above this value are required

for high performance thermoelectrics, and these thermopowers are indeed present in $CrSi_2$.

Of additional interest, these thermopowers are at very heavy dopings, which is important as the electrical conductivity usually increases substantially as carrier concentration is increased. Accordingly we find that this material may show good performance in the 900-1250 K temperature range if heavily doped n-type.

The discovery of a potentially good n-type thermoelectric is of importance given that in most cases, valence band dispersions are smaller than conduction band dispersions, so that p-type materials are generally easier to find – but any application requires *both* p-type and n-type materials. The large n-type thermopowers at these concentrations are generally a positive indicator for thermoelectric performance, since the electrical conductivity - a prerequisite for good performance – increases with carrier concentration. In addition, good thermopower is also present for hole-doping (not shown), with values above 200 μV/K at the hole concentration around $10^{21}/cm^3$. Materials showing good performance for both electron and hole doping are of particular value for applications such as exhaust waste heat recovery which require both p-type and n-type materials (ideally containing similar thermal expansion coefficients) to function. $CrSi_2$ has been already shown to be a material that can be doped both n-type and p-type [7,8] and is thus is potentially well suited for applications if it can be made with a high thermopower. We find this to be the case.

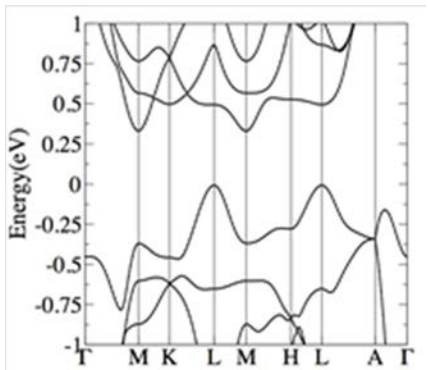

Figure 3. Calculated electronic band structure of $CrSi_2$.

We traced the origin of the large thermopowers for $CrSi_2$ to the band structure plot as shown in Figure 3. Both the valence and conduction bands have relatively small energy dispersion scales (the "heavy" bands), in line with the observation [9] that good thermoelectrics generally have electronic structure which changes significantly on the scale of k_BT, where k_B is Boltzmann's constant.

We are preparing a detailed technical report containing our findings for $CrSi_2$ and their scientific basis.

We have also continued work on Ni-doping in skutterudites, for which we previously did first principles calculations of a similar type to those reported above for $CrSi_2$. During the present quarter we collaborated with General Motors (Jihui Yang, supported by G.M. and DOE corporate agreement DE-FC26-04NT42278) and partners of G.M. to analyze new experimental data on this system. The experiments, which were motivated by our previous calculations, showed improvement in the thermoelectric performance of the Ni-doped samples relative to rare-earth filled iron antimonide. A bipolar effect was also found, which if mitigated could lead to a further improvement. A technical report detailing these findings is being prepared.

Status of FY 2012 Milestones

We are making progress towards our milestone of successfully predicting new thermoelectric compositions. We plan to study $AgGaTe_2$ and several related chalcopyrite structure materials for their potential for high temperature applications and in addition develop the ability to perform lattice dynamics calculations for increasingly complex systems. We also plan to explore the potential thermoelectric performance of the kesterite materials $Cu_2ZnSnSe_4$ and Cu_2ZnSnS_4, both composed of inexpensive and abundant elements.

Problems Encountered

No significant problems encountered this quarter.

Publications/Presentations/Awards

1. D. Parker and D.J. Singh, "Potential thermoelectric performance from optimization of hole-doped Bi_2Se_3", Phys. Rev. X **1**, 021005 (2011).
2. D. Parker, ORNL Materials and Chemistry Seminar, "From Heat to Electricity: Recent Theoretical Work on Thermoelectrics at Oak Ridge", December 14, 2011 (invited seminar).

References

1. P. Blaha, K. Schwarz, G. K. H. Madsen, D. Kvasnicka and J. Luitz, WIEN2k, An Augmented Plane Wave + Local Orbitals Program for Calculating Crystal Properties (Karlheinz Schwarz, Techn. Universitat Wien, Austria), 2001. ISBN 3-9501031-1-2.

2. G.K.H Madsen and D.J. Singh, "BoltzTraP: a code for calculating band-structure dependent quantities", Computer Physics Commun. **175**, 67 (2006).

3. Available from United States Geological Survey report on Chromium production,http://minerals.usgs.gov/minerals/pubs/commodity/chromium/mcs-2011-chrom.pdf.

4. C.B. Vining, "Thermoelectric properties of silicides", CRC Handbook of Thermoelectrics, D.M. Rowe, ed. 1995.

5. A.F. Ioffe, "Semiconductor Thermoelements and Thermo-electric Cooling", (Inforesearch: London) 1957.

6. The Wiedemann-Franz relation states that the electronic thermal conductivity $\kappa_{electronic}$ and electrical conductivity σ are related by $\kappa_{electronic} = L_0\sigma T$, where L_0 is the Lorenz number.

7. Z. J. Pan, L. T. Zhang and J. S. Wu, Scripta Materialia **56**, 245 (2007).

8. H. N. Zhu, K. Y. Gao and B. X. Liu, J. Phys. D: Appl. Phys. **33**, L49, (2000).

9. D. J. Singh, “Theoretical and computational approaches for identifying and optimizing novel thermoelectric materials”, Semiconductors and Semimetals **70**, 125 (2001).